POLYANILINE SORPTION OF RUTHENIUM

A Thesis
Presented to
The Academic Faculty

by

Allison M. Harbottle

In Partial Fulfillment
of the Requirements for the Degree
of Master in Science in the
School of Chemistry and Biochemistry

Georgia Institute of Technology
August 2016

POLYANILINE SORPTION OF RUTHENIUM

Approved by:

Dr. Jiří Janata, Advisor
School of Chemistry and Biochemistry
Georgia Institute of Technology

Dr. Lawrence Bottomley
School of Chemistry and Biochemistry
Georgia Institute of Technology

Dr. Nolan E. Hertel
School of Mechanical Engineering
Georgia Institute of Technology

Date Approved: July 25th, 2016

ACKNOWLEDGEMENTS

I would like to thank my parents, Becky and John, for their unconditional love and support through this process. I would not have made it this far without them. In addition, I would like to thank my boyfriend Chris for standing by me and supporting my decisions for our future. I am also thankful for the knowledge, leadership, and guidance that have been provided by my advisors Dr. Jiří Janata and Dr. Mira Josowicz. I could not have asked for a better set of advisors to shape me as a scientist and help me find my path in life. Lastly, I'd like to thank my graduate committee Dr. Jennifer Steeb, Dr. Angus Wilkinson, Dr. Lawrence Bottomley, and Dr. Nolan Hertel and fellow lab mates Erin Gawron, Steven Hira, Tomas Krizek, Alex Jonke, Malvina Kowalik, and Charles Wang for their advice and support throughout this process.

TABLE OF CONTENTS

LIST OF TABLES

Page

LIST OF FIGURES

Page

LIST OF SYMBOLS AND ABBREVIATIONS

b	Langmuir constant
C_e	Equilibrium constant of Ru ion
CV	Cyclic Voltammogram
EB	Emeraldine Base
ES	Emeraldine Salt
K_f	Freundlich capacity factor
K’	Rate constant for pseudo second order kinetics
N	Freundlich intensity factor
PANI	Polyaniline
PANI-B	Polyaniline after buffer condition
PANI-P	Polyaniline ($H_2PO_4^-$)
PANI-Ru	Polyaniline with Ru Sorbed
PAS	Photoacoustic Spectroscopy
PGM	Platinum Group Metals
q	Max occupancy of sorption sites on PANI
q_e	Sorption capacity of PANI in equilibrium state
q_t	Sorption capacity of PANI at time (t)
RVC	Reticulated Vitreous Carbon
SIA	Sequential Injection Analysis
TGA	Thermal Gravimetric Analysis
XPS	X-ray Photoelectron Spectroscopy

SUMMARY

The goal of this project was to determine if polyaniline would be an adequate matrix to sequester ruthenium from aqueous solutions. Ruthenium is a component of radioactive hazardous waste, and therefore developing a sorption method could provide an opportunity to lower costs and be more efficient. The sorption process of $RuCl_3$ in phosphate buffer by PANI powder chemically synthesized from phosphoric acid was spectrophotometrically monitored as function of time. It was determined that the sorption process follows the Langmuir and Freundlich isotherm models and their equation constants were evaluated. The rate constant averaged within the tested ruthenium concentration range ($7.9x10^{-5}$ to $1.2x10^{-3}$M) was experimentally determined to be $1.3x10^{-2}$ $g*mg^{-1}*min^{-1}$. The high R^2 value (0.99+) of the rate constant supports the pseudo-second order kinetics and is in agreement with chemisorption being the rate-controlling step. By conducting detailed studies we assigned the chemisorption to Lewis acid based interactions of the sorbent electron pair localized at the benzenoid amine ($-NH_2$) and quinoid imine (=NH) groups, with the sorbate, $RuCl_3$ in solution, as the electron acceptor. The stability of the interaction over a period of approximately a week showed that the presence of the Ru(III) in the PANI matrix reverses its state from emeraldine base to emeraldine salt resulting in a change of conductivity. The partial electron-donor based charge transfer is a slow process when compared to the sorption process involving Brønsted acid doping.

CHAPTER 1

INTRODUCTION

1.1 Overview of Ruthenium Separation Methods

Ruthenium is a member of platinum group metals (PGM) and has desirable chemical properties such as remarkable catalytic activity and stable electrical properties[1]. Unlike other PGM, it has many challenges such as slow ligand exchange reaction chemistry and tendency to hydrolyze. Ru-103 and Ru-106 are decay products found in spent nuclear fuel[2, 3] and prove to be some of the most hazardous components to the environment due to volatility concerns[4]. Low level radioactive waste generated from the uranium/plutonium purification process and from waste evaporation due to the PUREX process generate Ru-106 along with many other radionuclides such as Cs-137 and Sr-90[5]. The amount of ruthenium metal from irradiated nuclear fields is expected to become comparable to that of natural resources[6]. Finding an effective method to remove ruthenium from these nuclear waste areas could become an important resource for future demands of medical radioactive treatments due to the limited amount natural resources available. Additionally, radioactive ruthenium, such as Ru-106, is useful in medical devices for radiation treatment[7-10]. Developing a method to selectively collect Ru-106 from solution onto a solid substrate with subsequent elution would collect ample amounts raw material for medical devices such as radioactive seeds for cancer treatments[7, 10].

Many separation methods, are currently employed to extract precious metals from mixtures. These methods, however, prove to be expensive and lengthy due to multiple steps[11]. For this reason, adsorption methods are promising for the removal and recovery of precious and heavy metals[11]. The use of primary and secondary amine groups on ionic polymers to coat biomaterials as a biosorbent[11] or the use of chemicals

such as dipropylmethyl-2-(N,N-diisobutyl) acetamidoammonium iodide impregnated in resins[4] have been presented in the literature and allows for ~30mg /g and 6.25mg / g ruthenium to be collected, respectively. The goal of this project was to improve on the amount of ruthenium that could be collected and design a field device that is portable and easy to use for nuclear forensic applications of trace detection.

1.2 Polyaniline as a Sorbent

In the literature, polyaniline powder has successfully been used for sorbing heavy metals from effluents *e.g.* Cr(VI)[12, 13] and Hg(II)[14, 15] with the help of complexing agents such as humic acid[15]. The high radiation stability makes it an excellent sorbent for removal of radionuclides such as Cs-137[16] and Hg-203[14]. Kumar *et al.* was investigating the removal of Ru-106 ($t_{1/2}$ = 374d) from radioactive waste using PANI as an anion-exchanger[17]. The ability to form anionic halo-complexes with Pd(II), Ir(IV), Pt(IV), and Au(III) demonstrated the ion exchange capabilities of PANI for separations of noble metals[18]. The use of PANI for anion exchange separation of halides such as Cl^-, Br^-, and I^- was also previously investigated[19]. Interestingly, all these studies confirm that the sorption process of an analyte is controlled by protonation and doping of the polymer and by the oxidation state of the analyte. Because of the versatility of the polymer, PANI can be used for sorption of Pb(II) and Cd(II)[20] as well as Ag^+ ions[21] from aqueous solutions making it an ideal sorbent for environmental applications. In fact, sorption techniques are generally more effective for removal of trace levels compared to high concentrations of solute[21].

Polyaniline is unique due to its ability to undergo oxidation and reduction as well as acid-base chemistry and is a thermally stable polymer. Chemical polymerization of PANI in solution is the simplest method of preparation. The important factors for polymerization are concentration, type of acid dopant used, and oxidant to monomer

ratio which all can affect the size of the synthesized solid PANI granules. Type of acid dopant and concentration are also factors to consider when electrochemically depositing the polymer on an electrode surface. The acidic and basic forms of PANI in each oxidation state are shown in Figure 1.1. The fully oxidized form of PANI is known as pernigraniline and the fully reduced form as leucoemeraldine. Between these two oxidations states is the emeraldine form of the polymer. PANI has the ability to be protonated and deprotonated. The protonated emeraldine salt form of the polymer is the only electrochemically conducting form. The properties and morphology of the polymer can be tuned, making it the ideal matrix for a separation column[22-27].

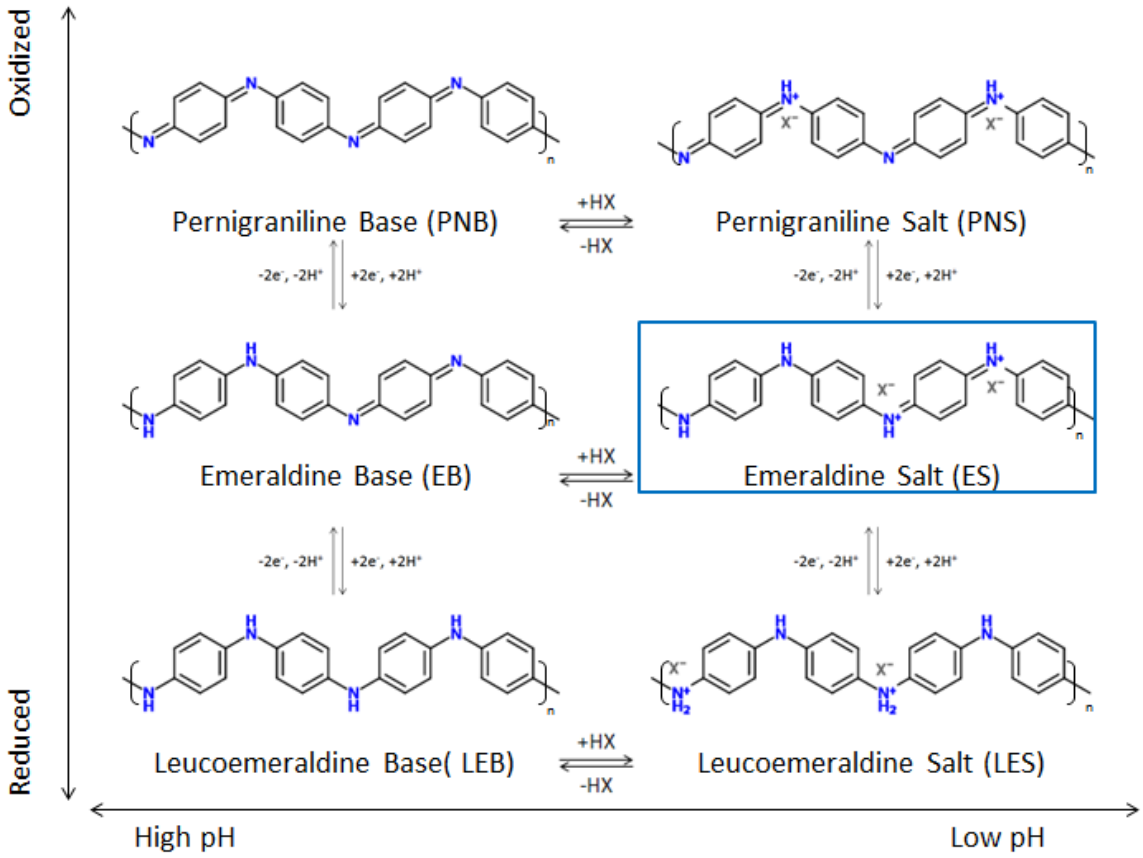

Figure 1.1. *Different Redox states possible in Polyaniline.*

Polyaniline is highly stable in strongly alkaline or acid media[28] and the effect of pH on

the Cs- or Ru-ion exchange properties of PANI was examined by varying the ratio of concentrated acid/base such as HNO_3/NaOH[16], or HCl/NaOH[17] in the pH range of 2-10. However, with these strong electrolytes, the pH and buffer capacity in mid-pH range cannot be controlled. Those studies showed that the uptake of Cs(I) or Ru(III) was the highest for pH 7-10. For this reason, PANI in a pH 7.0 solution with buffer capacity was used to have better control over the sorption process.

CHAPTER 2

SPECTROSCOPIC STABILITY OF RUTHENIUM COMPLEXES

2.1 Experimental Solution Preparation

The following complexes were tested for their stability in solution using UV-Vis absorption spectroscopy:

- Ruthenium (III) chloride hydrate ($RuCl_3 \bullet 3H_2O$ 97% purity Oakwood Chemical)
- Potassium pentachloronitrosylruthenate (II) (K_2RuCl_5NO Alfa Aesar)
- Potassium hexa-chlororuthenate (IV) (K_3RuCl_6 99.95% purity Alfa Aesar)
- Potassium aquapenta-chlororuthenate (III) ($K_2RuCl_5(H_2O)$ Aldrich)
- Potassium hyexacyanoruthenate (II) hydrate ($K_4Ru(CN)_6$ Strem)

All aqueous ruthenium solutions were made immediately before use. This is important to note because many ruthenium solutions were unstable over time. The stability of ruthenium complexes and corresponding acidic or basic media are presented in Table 2.1 and will be analyzed further in the following sections. A fully stable ruthenium complex in the specified solution with no spectral changes over time is denoted ‘S’. Relatively stable, denoted ‘RS’ is defined as a change of spectral absorbance with time but becomes stable within a week. Combinations of ruthenium complex and solvent that never reach stability are denoted ‘NS’ and not tested combinations are denoted ‘NT’.

Table 2.1. *Stability of Ruthenium Complexes in Acidic and Basic Media.*

	0.1M HCl	**1M HCl**	**0.1M $HClO_4$**	**1M $HClO_4$**	**1M HBF_4**	**1M NaOH**
$RuCl_3 \bullet 3H_2O$	RS	RS	NS	NS	NS	NS
K_2RuCl_5NO	S	S	S	S	NS	NS
K_3RuCl_6	NS	NS	NS	NS	NS	NS
$K_2RuCl_5(H_2O)$	NS	NS	NS	NS	NS	NS
$K_4Ru(CN)_6$	S	S	S	S	NT	NT

Acid stock solutions (0.1M and 1M) of hydrochloric acid (HCl 38% w/v EMD), perchloric acid ($HClO_4$ 70% w/v Macron), and tetrafluoroboric acid (HBF_4 48% w/v Strem) were prepared and stored in sealed volumetric flasks. A basic solution of 1M sodium hydroxide (NaOH Fisher) was also prepared and stored in a sealed volumetric flask. Various buffer solutions were prepared to be tested for applicability towards the system. Neutral buffers tested (between pH 6-7 at 0.1M concentration) include 3-(N-morpholino)propanesulfonic acid (MOPS 99% purity Aldrich), 2-(N-morpholino)ethanesulfonic acid (MES Aldrich), tris(hydroxymethyl)-aminomethane ($C_4H_{11}NO_3$ 99.8% purity Acros Organics), sodium acetate ($CH_3COONa•3H_2O$ Fisher and CH_3COOH 99.8% purity Fisher), and phosphate ($NaH_2PO_4•H_2O$ 98.9% purity Fisher and Na_2HPO_4 99.8% J.T. Baker). Ultraviolet Visible Spectroscopy (UV-Vis) measurements were performed using a Shimadzu UV-3101PC double beam instrument with a 1-cm path length in the range of 200-800nm.

2.2 Stability of Ruthenium Complexes in Acidic and Basic Media

Ruthenium complexes were initially tested for their stability in acidic solution using absorbance spectroscopy. From the literature, it was shown that ruthenium undergoes slow ligand exchange[29] in hydrochloric acid solution and makes various aqua-chloro complexes[30, 31].

It was determined that K_3RuCl_6 and $K_2RuCl_5(H_2O)$ underwent very slow ligand exchange and formation of aqua-chloro complexes in both acidic and basic media. The stability of these two complexes in 1M HCl is shown in Figure 2.1. Initially the two complexes are different in terms of the intensity of the peaks at approximately 220nm, 270nm, 380nm, and 480nm indicating that there are different ratios of aqua-chloro complexes in solution. Within 48 hours, however, both complexes show almost identical

absorbance spectra. Both complexes in 1M HCl media continued to change spectrally over the 6 day period it was monitored (additional spectra not shown).

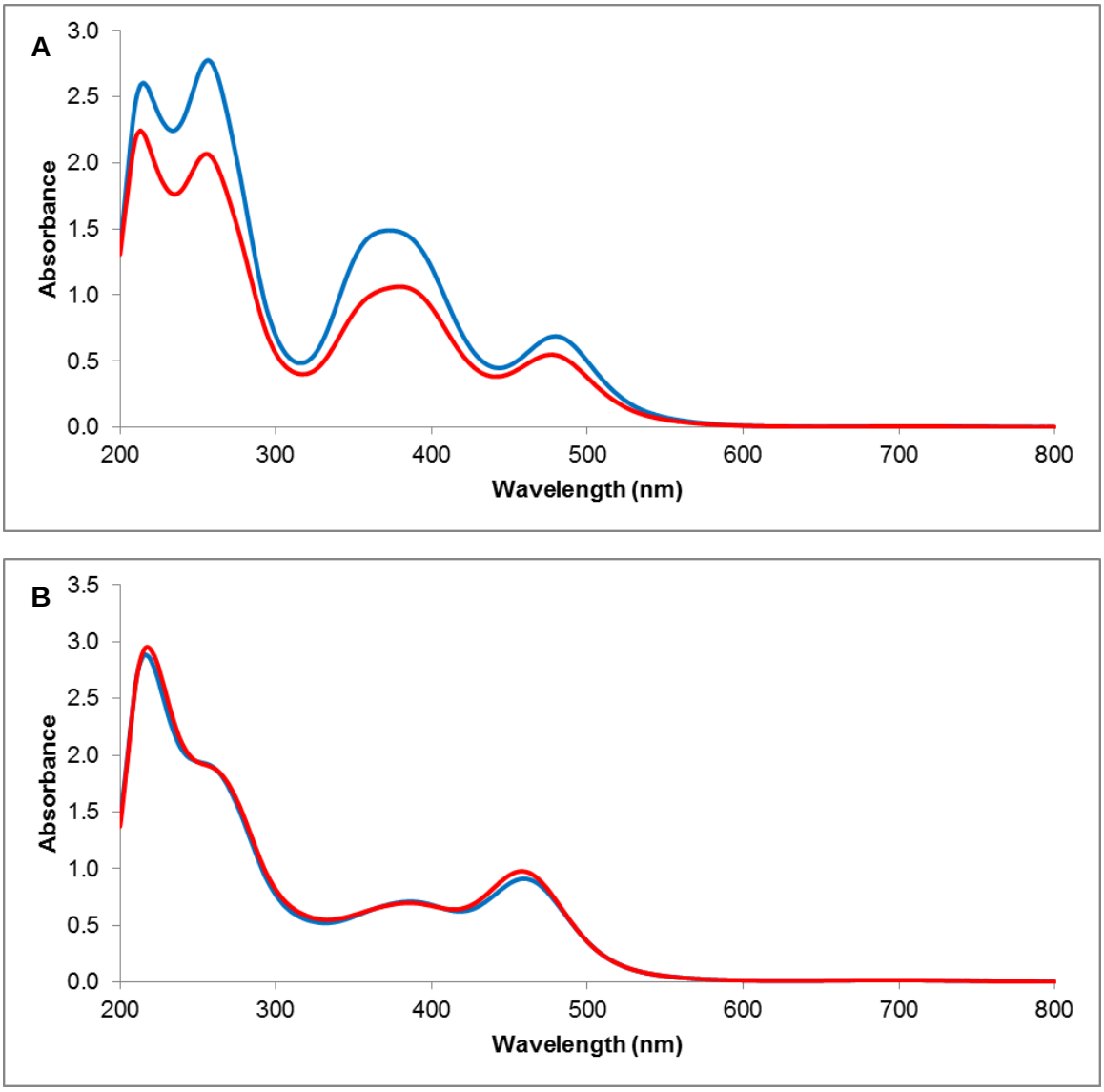

Figure 2.1. *Stability of K_3RuCl_6 (blue) and $K_2RuCl_5(H_2O)$ (red) in 1M HCl solution. Initial UV-Vis spectra (A) and spectra after 48 hours (B).*

The $K_4Ru(CN)_6$ complex proved to be very stable in acidic media, however was problematic due to high absorbance signal in the range of 200-220nm. Due to the high stability of this complex, it was hypothesized that it would not undergo ligand exchange and would not react easily with the amine and imine sites on the PANI. Therefore, it was not further considered as a model ruthenium complex.

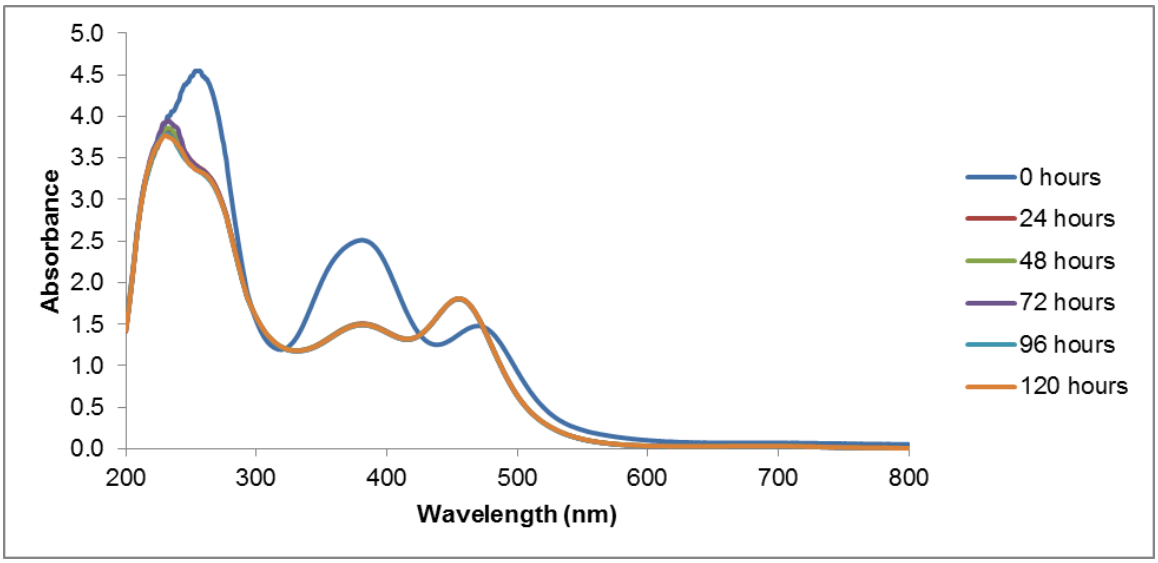

Figure 2.2. *UV-Vis spectral absorbance of 0.603mM $RuCl_3$ in 1M HCl over a 5 day period.*

The $RuCl_3$ complex was monitored over a 5 day period in a solution of 1M HCl. Initially $RuCl_3$ transitioned between aqua-chloro complexes in solution and the absorbance spectra changed rapidly, but found a stable point within 24 hours without major futher spectral changes occuring after a 24 hour period. The UV-Vis spectra of a 0.603mM $RuCl_3$ solution in 1M HCl is shown above in Figure 2.2. Due to its eventual stability in solution, $RuCl_3$ was chosen for further testing in varying pH ranges.

The only compound tested with relatively constant stability in acidic media was K_2RuCl_5NO. This ruthenium compound showed minimal changes in both 0.1M $HClO_4$ and 1M HCl. Figure 2.3 shows the linear range of K_2RuCl_5NO in 0.1M $HClO_4$ with a molar absorptivity coefficient of 21469 $L*cm^{-1}*mol^{-1}$ in the range of 0 to $1x10^{-4}$M. Although a limited linear concentration range for absorsorbance measurements was experimentally determined, K_2RuCl_5NO was the second ruthenium complex selectred for further analysis. It can be noted that all complexes tested in 1M NaOH were not stable with time (raw data not shown). Therefore, it was concluded that basic media was not appropriate for further sorption and desorption studies using ruthenium complexes as long as UV-Vis absorption was the main method for analysis.

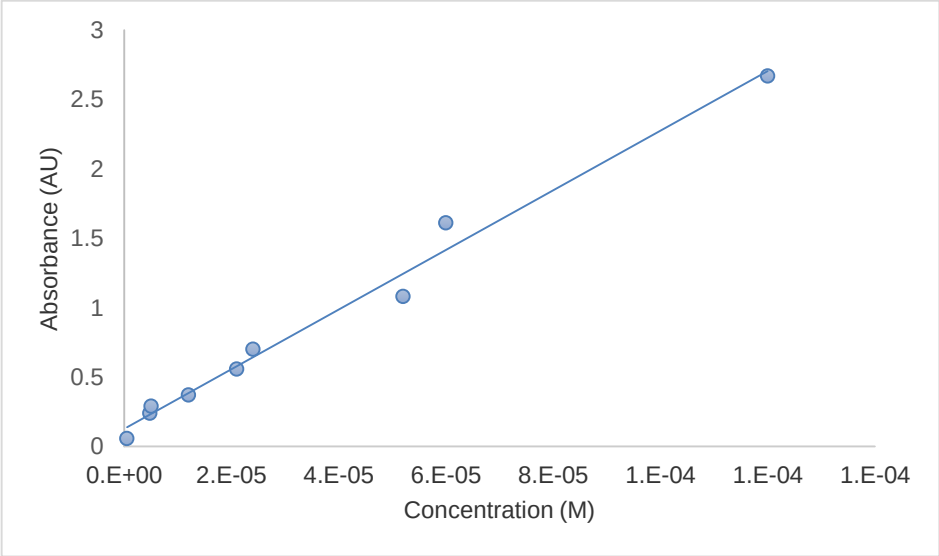

Figure 2.3. *UV-Vis absorbance calibration curve of K_2RuCl_5NO complex in 0.1M $HClO_4$ measured within 24 hours of solution preparation.*

2.3 Stability of Ruthenium Complexes in Buffered Media

Phosphate buffer at pH 7.0 produced an absorbance spectra similar to that of water with no signatures that could potentially interfere with ruthenium measurements. All other buffers tested showed a strong absorbance signal in the range of 200-250nm which interfered with many of the ruthenium complexes tested, and therefore were not chosen.

Three complexes, K_2RuCl_5NO, $RuCl_3$, and K_3RuCl_6 showed UV-Vis spectral stability in phosphate buffer. Although showing relative stability in phosphate buffer, K_3RuCl_6 was not considered due to its instability in acidic media. Calibration curves for both K_2RuCl_5NO and $RuCl_3$ complexes in 0.1M phosphate buffer at pH 7.0 were recorded and are shown in Figures 2.4 and 2.5 with molar absorptivities of 9626 and 1996$L*cm^{-1}*mol^{-1}$, respectively. The $RuCl_3$ compound had a slightly larger linear concentration range for absorbance measurements and was therefore selected as the model compound for sorption. Additionally, $RuCl_3$ is more representative of the ruthenium in the environment due to its ability to form aqua-chloro complexes[30].

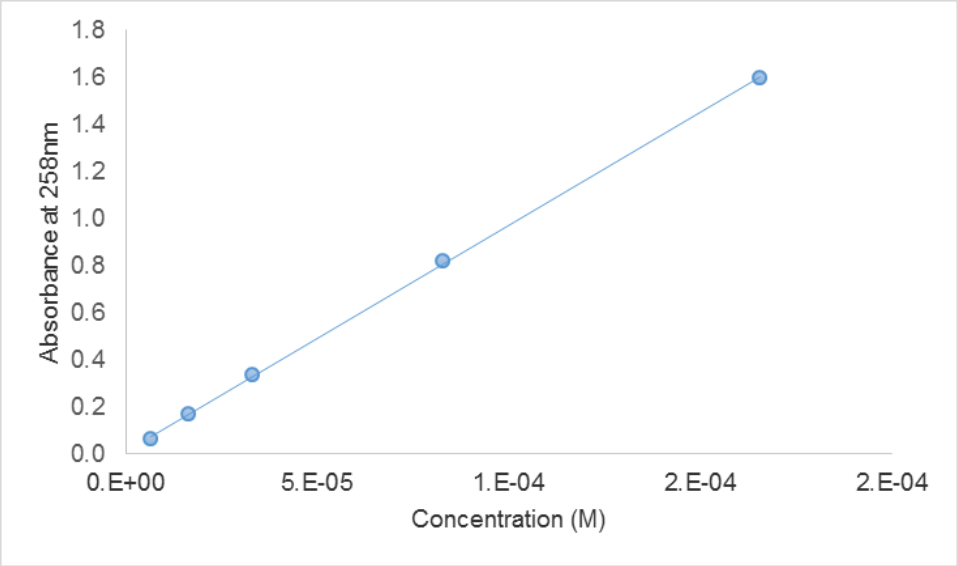

Figure 2.4. *UV-Vis calibration curve for K_2RuCl_5NO complex dissolved in 0.1M phosphate buffer (pH 7).*

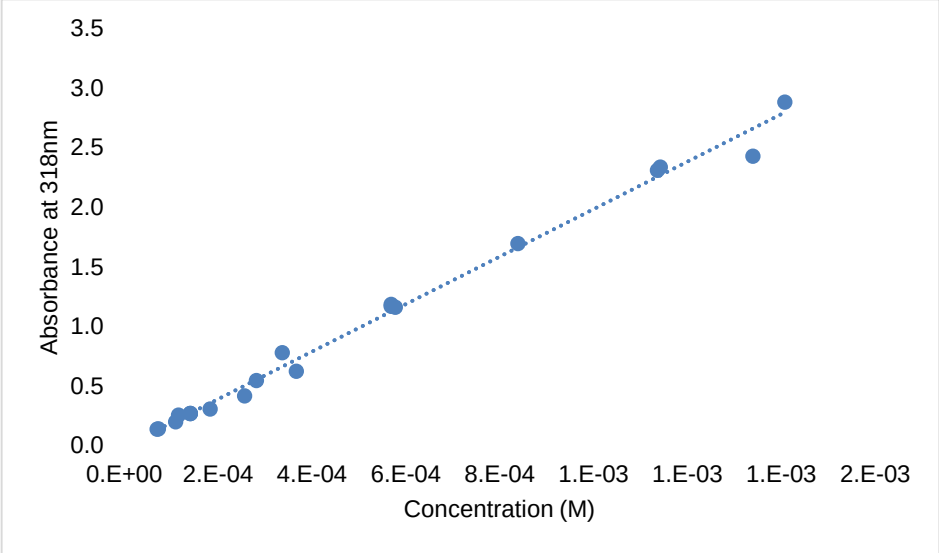

Figure 2.5. *UV-Vis calibration curve for $RuCl_3$ complex dissolved in 0.1M phosphate buffer (pH 7).*

The stability of a $1.16x10^{-4}$M $RuCl_3$ solution in 0.1M phosphate buffer was monitored over a month via UV-Vis absorption without a shift in the peaks or decrease in absorbance intensity and it presented in Figure 2.6. The λ_{max} at 318nm is due to neutral $RuCl_3$ species[32, 33]. The $RuCl_3$ complex was previously used in sorption studies using

PANI[17]. However, sorption studies with PANI have not been performed to our knowledge within a controlled pH buffered media.

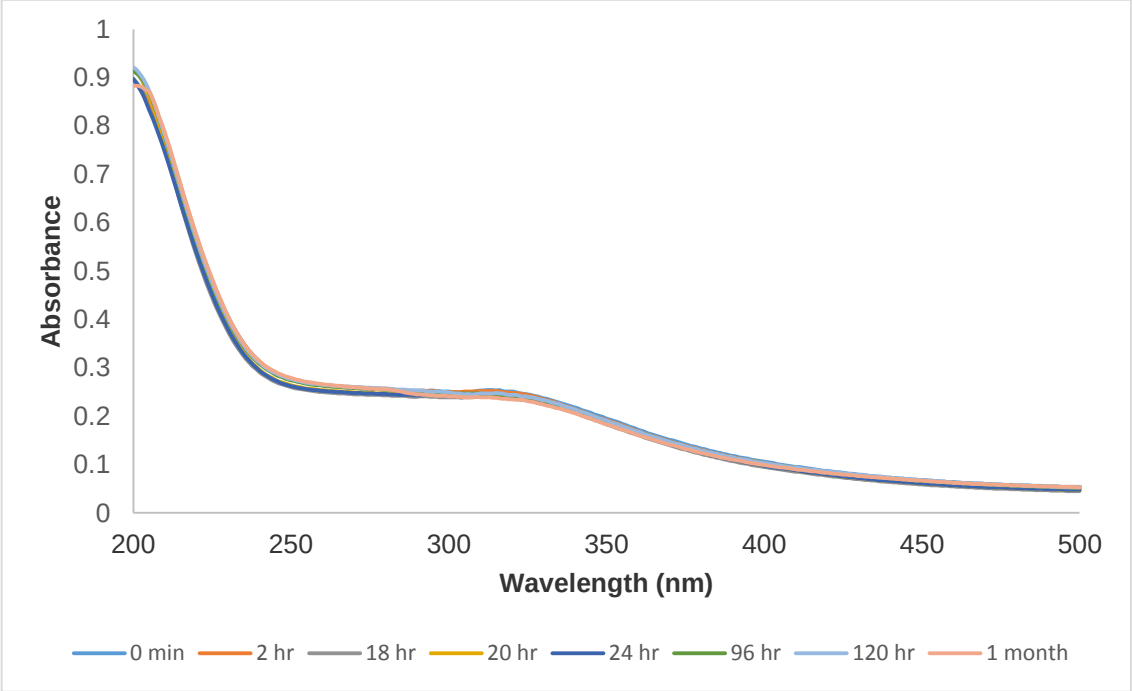

Figure 2.6. *Stability of 1.16x10^{-4}M $RuCl_3$ solution in 0.1M phosphate buffer (pH 7.0) monitored over a one month period.*

CHAPTER 3

CHEMICAL AND ELECTROCHEMICAL POLYMERIZATION OF POLYANINE

3.1 Solution Preparation for Polyaniline Synthesis

Aniline ($C_6H_5NH_2$ 99+% purity Alfa Aesar), sodium phosphate monobasic ($NaH_2PO_4 \cdot H_2O$ 98.9% purity Fisher Scientific), sodium phosphate dibasic anhydrous (Na_2HPO_4 99.8% purity J.T. Baker), ammonium persulfate ($(NH_4)_2S_2O_8$ 98+% purity Aldrich), and phosphoric acid (H_3PO_4 85% w/v Amresco) reagents were analytical grade and used as received.

All solutions were prepared using deionized water (18MΩ) and stored in sealed vials. A pH 7.0 solution of 0.1M phosphate buffer was prepared using 39mL of 0.2M Na_2HPO_4 and 61mL of 0.2M $NaH_2PO_4 \cdot H_2O$. Buffer pH was verified using a PHM240 pH/Ion Meter (Radiometer Analytical). For polyaniline synthesis, stock solution of acid (3M H_3PO_4), oxidant (0.2M $(NH_4)_2S_2O_8$ in 3M H_3PO_4) and monomer (0.2M aniline in 3M H_3PO_4) were prepared.

3.2 Synthesis of Polyaniline Powder and Thin Film

The polymerization process for PANI occurs through a mediated electron transfer process[34]. Although it is difficult to polymerize PANI from H_3PO_4[27], the phosphate anion was well suited for our application. Polymerization from H_3PO_4 allows PANI to have a higher buffer capacity[24].

Polyaniline was synthesized by adding 100 mL of $(NH_4)_2S_2O_8$ stock solution drop-wise over a period of 3-4 hours to a 500 mL aniline stock solution while stirring and cooling (5-10°C) using an ice bath[26, 35]. In the same reaction vessel, thin films of polyaniline were also polymerized on a quartz microscope slide. The PANI sorbent surface chemically polymerized on the quartz slide was removed from the reaction vessel and washed with deionized water and used for spectrophotometric

characterization. After synthesis, the remaining reaction mixture was immediately filtered by vacuum using a Buchner funnel. The filtrate was first rinsed with DI water, and then with methanol until solution remained clear signaling the removal of oligomers. Finally, the blue/black colored powder of PANI ($H_2PO_4^-$), PANI-P, was conditioned in 0.1M phosphate buffer (1 liter) for 24 hours and then filtered again. The obtained phosphate buffer washed material after buffer conditioning, PANI-B (Figure 3.1), was oven dried overnight at 70°C and stored in a sealed vial until further use.

Figure 3.1. *PANI-B powder chemically polymerized*

3.3 Polyaniline Deposition on Solid Support

Reticulated vitreous carbon (RVC), also known as carbon foam, provides a high surface area due to the porous nature of the material. A thick film of PANI can be deposited on a RVC solid support and placed in a separation column. Applications of constructing a sequential-injection analysis (SIA) system for portable sorption and detection of ruthenium could be possible using this material. PANI on an RVC support has been used in the literature as an electroanalytical technique to collect metal ions from solution[36]. It can be hypothesized that combining electrochemical techniques with

the sorption process may even provide higher sorption capacity of ruthenium by the PANI polymer.

Cylindrical pieces of RVC were cut into cylinders with a0.5cm diameter and 5cm length. The RVC was evacuated in 1M H_2SO_4 for 30min. This was to ensure that all pores were fully wetted before any electrochemical measurements were made[36]. An electrical contact was made to the top of the RVC with a Pt wire and carbon tape. The RVC was activated electrochemically by cycling in 1M $H_2S{+}{+}O_4$ from 0V to +1.4V for 20 cycles at 50mV/sec using a Pt cage counter electrode vs a Ag/AgCl reference electrode. RVC activation can be seen in Figure 3.2.

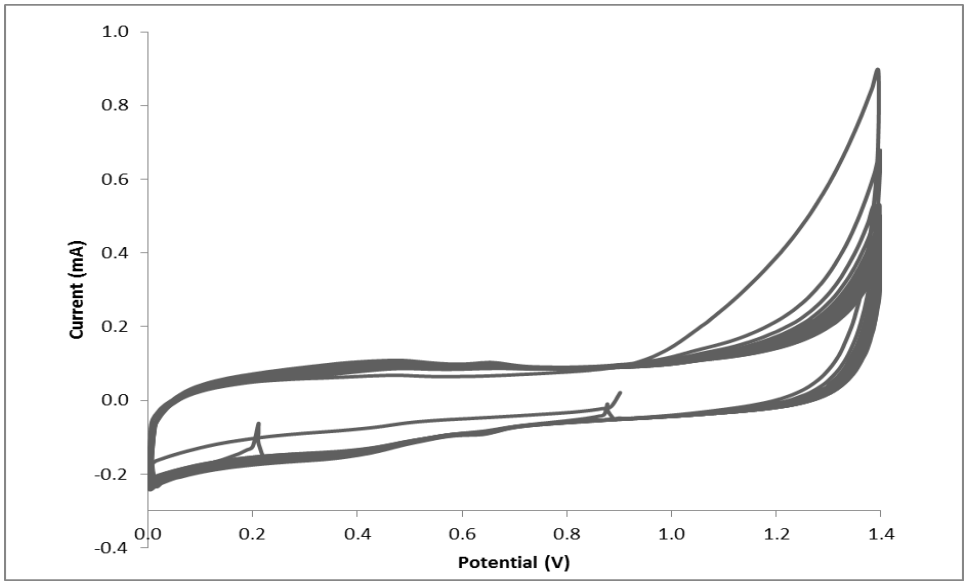

Figure 3.2. *Activation of RVC in 1M H_2SO_4 using cyclic voltammetry*

In order to create nucleation sites on the carbon, polyaniline was chemically polymerized on the RVC surface in three steps. (1) RVC was evacuated in a solution of 0.2M $(NH_4)_2S_2O_8$ in 3M H_3PO_4 for 30 minutes. (2) RVC was then evacuated in a solution of 0.2M aniline in 3M H_3PO_4 for 30 minutes to begin the polymerization process. (3) To ensure the elimination of oligomers on the surface, the RVC was again evacuated in a solution of 0.2M $(NH_4)_2S_2O_8$ for 30 minutes and then rinsed gently with DI water. All

solutions were prepared in H_3PO_4 to help control the morphology of PANI allowing for a more open polymer structure[34].

To obtain a thicker film of PANI, an electrical contact was again made with the top of the RVC with a Pt wire and carbon tape. A baseline cyclic voltammogram (CV) was performed in 1M H_3PO_4 to analyze the chemically deposited film on the surface as seen in Figure 3.3. PANI was then electrochemically deposited on RVC by running a CV in a solution of 0.2M aniline in 3M H_3PO_4 from -0.4V to +1.0V for 50 cycles at 25mV/sec using a Pt cage counter electrode against a Ag/AgCl reference. Due to the thickness of the film and the relatively fast scan rate of 25mV/sec, no features of PANI were present during the deposition process as is seen in Figure 3.4.

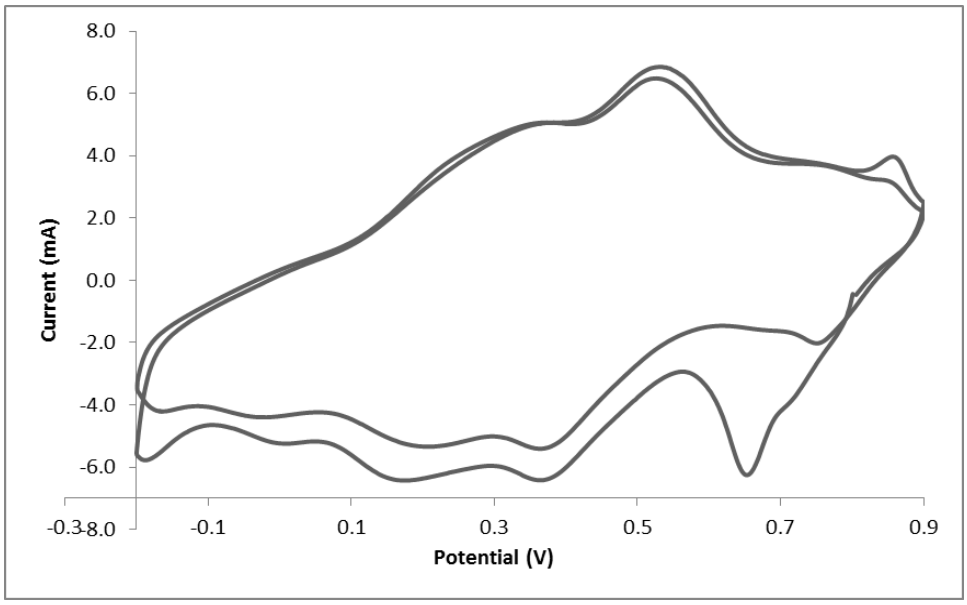

Figure 3.3. *CV of chemically polymerized PANI on RVC surface in 1M H_3PO_4*

After electrochemical deposition, the PANI film was characterized in 1M H_3PO_4 via CV in the range of -0.2V to +0.9V for 2 cycles at 1mV/sec. The slow scan rate was needed in order to gain visualization of the PANI features. To remove any additional oligomers on the surface that could dissolve into solution and interfere with future absorbance measurements, the film was cycled in basic solution (1M NaOH) and then

cycled again in 1M H_3PO_4. The two CV's of the RVC electrode performed in 1M H_3PO_4 before and after cycling in 1M NaOH are shown in Figure 3.5. RVC electrodes were rinsed with DI water and allowed to dry after polymerization and conditioning of the film.

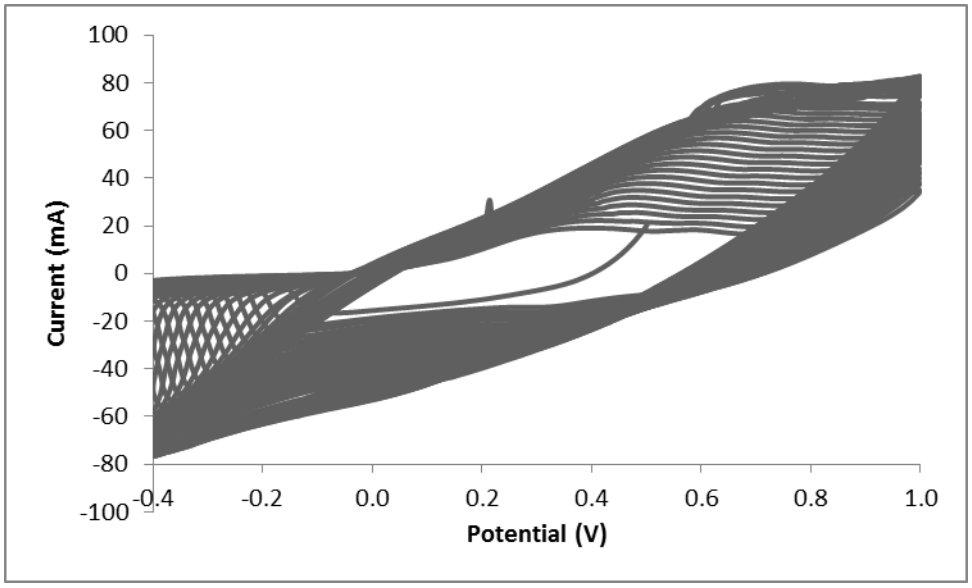

Figure 3.4. *Electrochemical deposition of PANI on RVC through cyclic voltammetry*

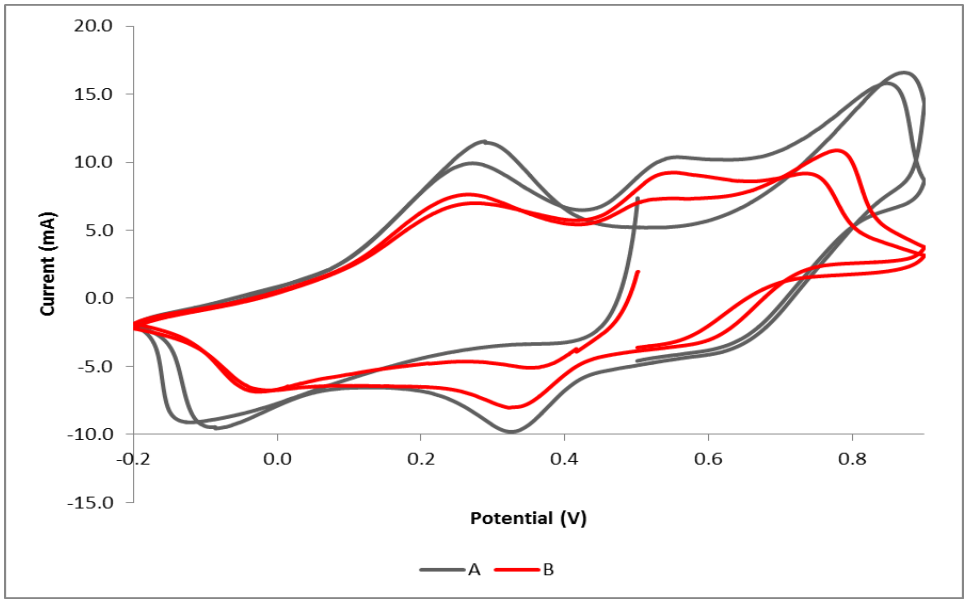

Figure 3.5. *CV of PANI on RVC in 1M H_3PO_4 before (A) and after (B) being conditioned in 1M NaOH.*

On the reverse scan in Figure 3.5, three reduction peaks can be seen at approximately 0.65V, 0.3V, and -0.1V. The reduction peaks at 0.65V for the leucoemeraldine to emeraldine transition and at -0.1V for the emeraldine to pernigraniline transition are typical for PANI. For PANI, this process is reversible and the oxidation peaks on the forward scan are found at approximately 0.3V and 0.8V. The peak at 0.3V on the reverse scan and at 0.55V on the forward scan can be attributed to cross-linking due to the nitrenium aniline cation and the nitrenium of the polymer[37]. Preliminary experiments using a lower concentration of acid during polymerization resulted in a higher middle peak and therefore a higher concentration of acid (3M H_3PO_4) was used to reduce cross-linking. Reducing the middle peak is important in order to not lower the conductivity of the polymer[37]. When comparing the finalized polymer with the original initial chemical polymerization (Figure 3.3) on RVC, it's clear that the middle peak is drastically reduced. It was concluded that the combination of chemical and electrochemical polymerization on RVC resulted in a thicker and more conducting film.

CHAPTER 4

RUTHENIUM SORPTION STUDIES USING UV-VIS ABSORBANCE SPECTROSCOPY

4.1 Overview of $RuCl_3$ Sorption by Polyaniline

Preliminary experiments using PANI as a matrix to collect ruthenium from low-level waste has been presented in the literature[17]. Lewis acids, such as $FeCl_3$, $RuCl_3$, or $SnCl_4$, are common oxidizing agents transforming neutral PANI polymer chains into poly-cations and can be prepared both in suspension (e.g. nitromethane) and in solution (e.g. 1-metyl-2-pyrrolidinone)[38-44]. However, Lewis acids are not usually strong oxidizing agents compared to the partially oxidized emeraldine salt (ES) form of the PANI. In that case, during an interaction a partial charge transfer process is expected, but not a full redox reaction. Thus, the electron transfer takes place between the $RuCl_3$ acting as a Lewis acid, and the amine/imine nitrogen sites of the emeraldine form acting as a Lewis base[45]. Up to now, the majority of the sorption research of PANI focused on the Brønsted equilibrium and on the protonation of PANI and neglecting the Lewis acid type interactions[35, 46, 47].

Polyaniline as an ion exchanger exhibits a strong dependence on pH[48-51], oxidation state[51, 52] and water content[51, 53-55]. The objective of this study was to investigate the uptake of Ru(III) in a pH 7.0 phosphate buffer solution. It was important for this study to be done at neutral pH to mimic environmental conditions for further applications. Furthermore, in order to improve the pH stability of the PANI sorbent, phosphoric acid was chosen as the dopant because it has buffer capacity over wide pH range. Polyaniline polymerized chemically from phosphoric acid yields a high molecular weight product that is important for the sorbent stability in solution. The aim of this study was to determine the extent of ruthenium uptake by PANI. A general schematic of the $RuCl_3$ interaction with PANI is presented in Figure 4.1 below. The sorption method study

presented here is important for collection of ultra-trace amounts of specific metal ions in aqueous systems.

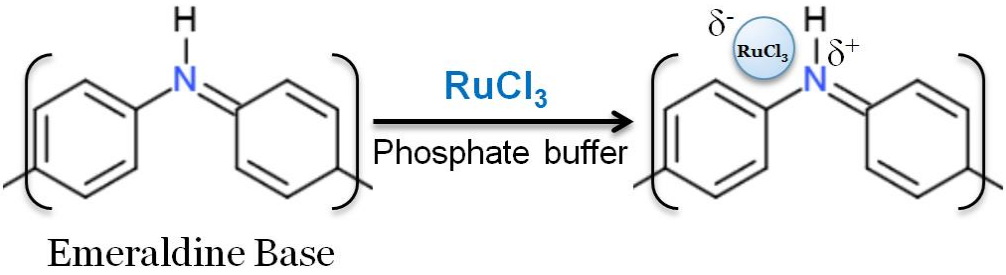

Figure 4.1. *Scheme of Lewis Acid-Base $RuCl_3$ interaction with PANI.*

The complete physical characterization of the Ru(III) sorption process by PANI was carried out using UV-Vis absorption, photoacoustic spectroscopy (PAS), resonance Raman spectroscopy, X-ray photoelectron spectroscopy (XPS) and by thermogravimetric analysis (TGA). Concentration of ruthenium solutions was limited by the linear absorbance range for UV-Vis spectroscopy.

4.2 Experimental

Prior to Ru(III) sorption, a control experiment was performed to ensure the optical stability of the PANI-B sorbent in buffer solution. The general sorption procedure for ruthenium can be described briefly by the following three steps: (1) A 10mL solution of $RuCl_3 \cdot 3H_2O$ (between $4x10^{-4}$ to $1.2x10^{-3}$M) in 0.1M phosphate buffer was added to 0.5g of dried PANI-B powder and continuously stirred. (2) The solution mixture was vacuum filtered through a Pyrex Buchner funnel (10-15μm pore size fritted disc) and the UV-Vis absorbance of the $RuCl_3$ was measured in the filtrate. (3) Immediately following, the ruthenium filtrate was returned to the vial and mixed with the filtered precipitate, PANI-Ru. The three steps were repeated ~5 times at different time intervals between 0-24 hours.

Polyaniline films on quartz slides were first conditioned to pH 7.0 in 0.1M phosphate buffer for 24 hours and then placed in a solution of 0.98mM $RuCl_3 \cdot 3H_2O$ in 0.1M phosphate buffer for an additional 24 hours.

4.3 UV-Vis Study of Polyaniline

The UV-Vis spectrum of a polyaniline film polymerized on quartz from 3M H_3PO_4 solution with a $(NH_4)_2S_2O_8$ oxidant to aniline monomer ratio of 1:5 is shown in Figure 4.2 (curve I). This spectrum shows two broad absorption bands with λ_{max} at 358nm due to the π-π* transition associated with self-localized electronic states of the double bond centered on the benzenoid (B) and quinoid (Q) rings and at 809nm due to the localized polaron-π*. The observed bands are consistent with the protonated state of the PANI in the ES form. After being in contact with phosphate buffer for 24 hours, peaks are blue shifted to λ_{max} at 334nm and an exciton n-π* transition of the non-bonding nitrogen lone pair to the conduction (π*) band at 668nm is present. In addition a weak shoulder appears at 430nm and could be due to the presence of a small localized semiquinone population in the film[56]. Hence, the energy of the n-π* transition increases while the energy decreases for the π-π* transition. The intensity increase of the band at 334nm can possibly be explained by the fact that the quinoid units are stabilized under this condition. Further equilibration in 0.1M phosphate buffer with 0.98mM $RuCl_3.3H_2O$ (PANI-Ru) causes a further small blue shift of the π-π* to 320nm and a larger blue shift of the n-π* transition to 620nm. The observed loss of the weak shoulder at 430nm and the blue shift of the π-π* transition allows assignment of this change in energy to a partial charge transfer interaction between $RuCl_3$ (Lewis acid) and the amine/imine centers of the benzenoid units (Lewis base). The shifting of the band from 668nm to 620nm is evidently due to the strength of the donor-acceptor interaction resulting in the partial oxidation of the emeraldine form.

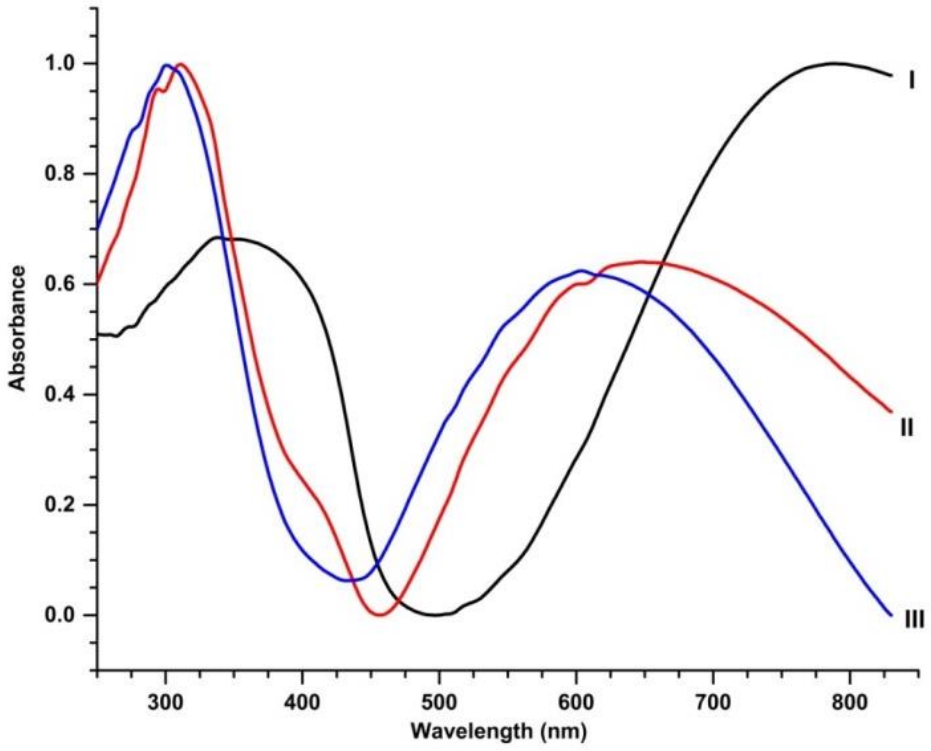

Figure 4.2. *UV-Vis spectra of polyaniline film chemically prepared on quartz slide and recorded in air after drying: (I) after synthesis in 3M H_3PO_4 (PANI-P), (II) after one day equilibration in 0.1 M phosphate buffer at pH 7.0 (PANI-B), and (III) after one day equilibration in 0.98mM $RuCl_3.3H_2O$ in the same buffer (PANI-Ru).*

4.4 Spectrophotometric Determination of Ruthenium Sorption

The stability of PANI-B in phosphate buffer allowed us to study of ruthenium uptake by PANI-B and was initiated by recording optical spectra of $RuCl_3 \bullet 3H_2O$ in phosphate buffer. In Figure 4.3, the absorbance of 10^{-4}M $RuCl_3$ in phosphate buffer shows only one broad peak at λ_{max}=318nm that was also reported for neutral ruthenium (III) chloride complexes[32, 33]. The buffer solution absorbs practically no light (like deionized water) in the wavelength region tested.

The spectrum of $RuCl_3$ in buffer remained unchanged over a period of one month, as was shown in Figure2.6. This high stability in the electronic transition peak of ruthenium reveals that the nature of this transition does not depend on buffer solution.

The absorptivity at λ_{max} was determined to be 2587.2 $L*mol^{-1}*cm^{-1}$ in the concentration range of $7.9x10^{-5}$ to $1.2x10^{-3}$M with a standard deviation of 1.01µg/mL. Upon contact of PANI-B with $RuCl_3$ in phosphate buffer solution, the intensity of λ_{max} decreased with time due to sorption (see Figure 4.3). The concentration of ruthenium remaining in the filtrate was calculated using the absorptivity coefficient.

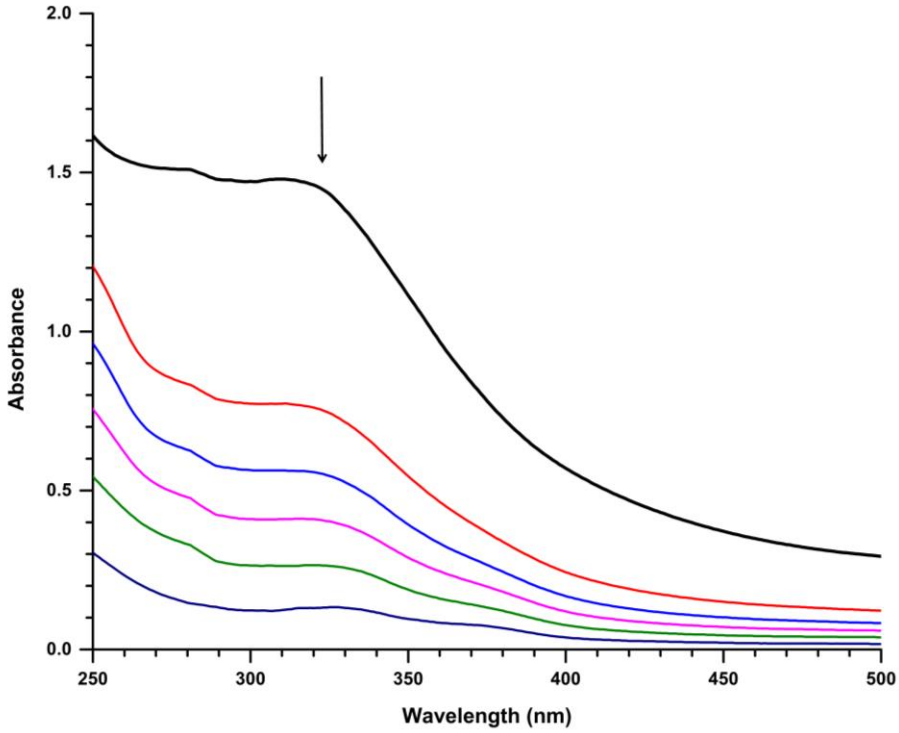

Figure 4.3. *Decrease in absorbance with increase of contact time of $RuCl_3$ ($7.19x10^{-4}$M in 0.1M phosphate buffer) with PANI at t=0 minutes, 30 minutes, 1 hour, 2 hours, 4 hours, and 24 hours.*

The sorption capacity of PANI was evaluated by monitoring the change in absorbance of $RuCl_3$ aliquots with increasing contact time to PANI-B (see experimental section). The amount of ruthenium sorbed was monitored over a period of 24 hours at different initial concentrations (Figure 4.4). Ruthenium sorption using this method, although not better than other methods, is on par and has room for improvement.

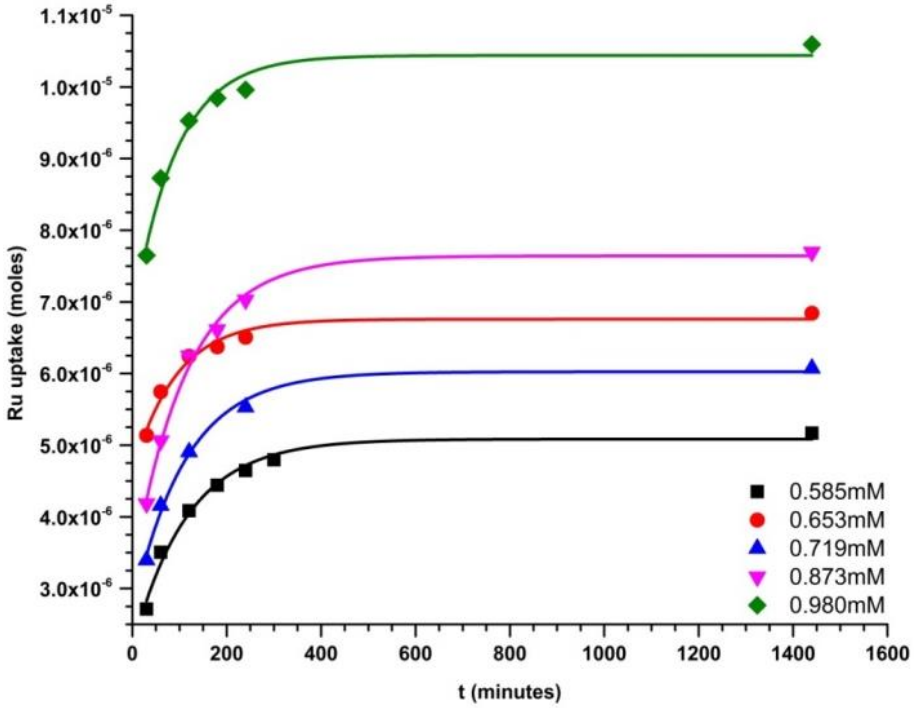

Figure 4.4. *Influence of PANI contact time on ruthenium sorption at different initial concentrations of $RuCl_3 \bullet 3H_2O$ in phosphate buffer.*

The initial removal of ruthenium by PANI-B increased rapidly within the first two hours and reached saturation within one day. No further sorption took place once the final capacity of the sorbate was reached. In order to identify the relationship between the amount of Ru(III) in the bulk solution and sorbed on PANI the experimental data were fitted into the Langmuir (Eq. 1) and Freundlich (Eq. 2) isotherms[12, 13, 57]:

$$\frac{C_e}{q_e} = \frac{C_e}{q} + \frac{1}{qb} \quad \text{..... (1)}$$

$$\log(q_e) = \frac{1}{n}\log(C_e) + \log(K_f) \quad \text{..... (2)}$$

where C_e (mg*L^{-1}) is the equilibrium concentration of ruthenium ion, q_e (mg*g^{-1}) is the sorption capacity of PANI in the equilibrium state, q is the maximum occupancy of sites, b is the Langmuir constant that reflects the energy constant of sorption between PANI and Ru(III), K_f is the Freundlich capacity factor, and n is the Freundlich intensity factor.

Table 4.1 shows the calculated constants from isotherm plots. The Langmuir isotherms are presented in Figure 4.5.

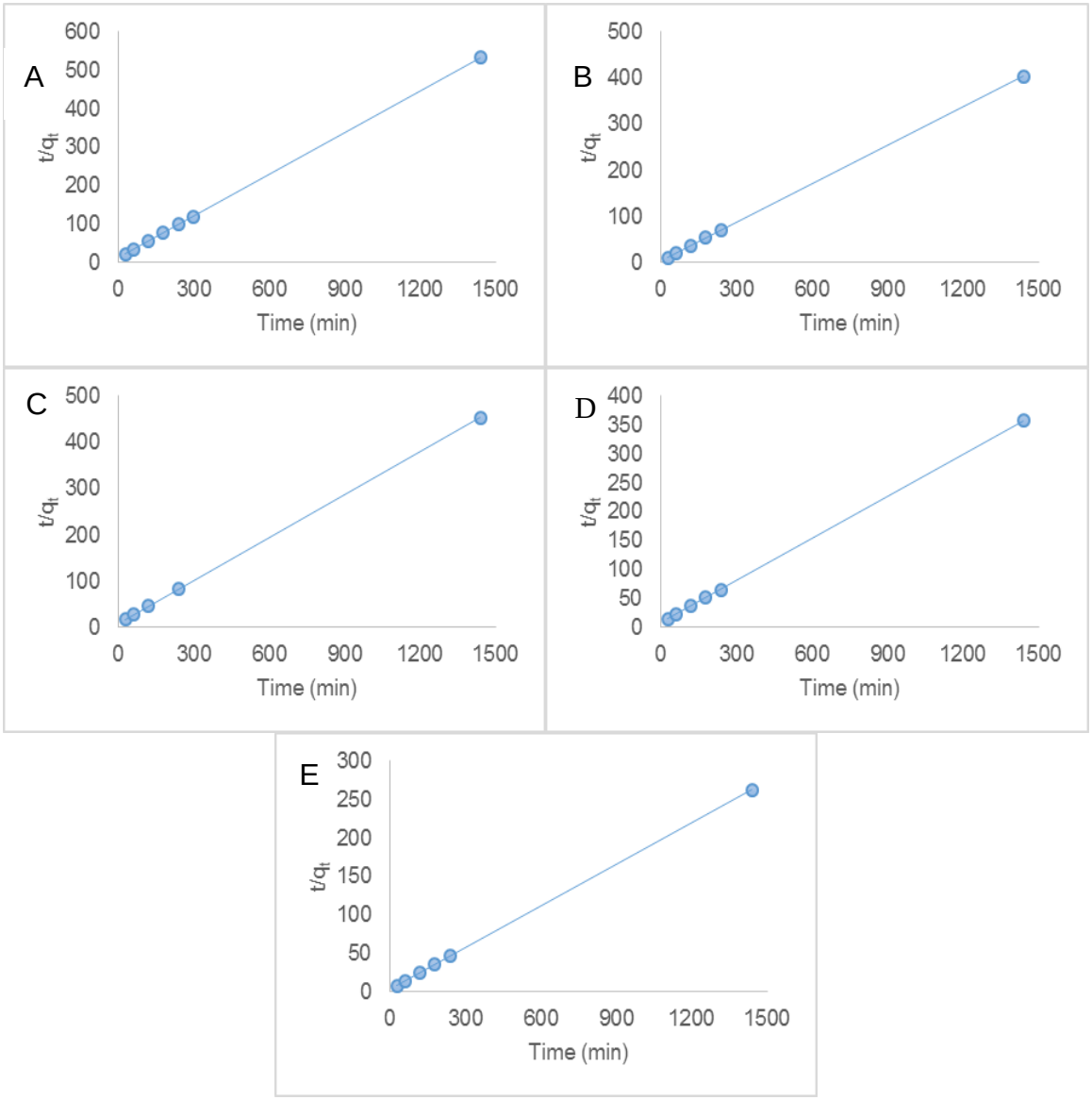

Figure 4.5. *Langmuir isotherm plots for $RuCl_3$ in 0.1M phosphate buffer (pH 7.0) in the following concentrations: (A) 0.585mM (B) 0.653mM (C) 0.719mM (D) 0.873mM and (E) 0.980mM*

The regression coefficients (R^2) for both isotherms were 0.99 suggesting a good model fit. The value of *n* between 1 and 10 indicates favorable adsorption[12]. For systems where there is a structurally homogeneous sorbent with a finite number of sites, the Langmuir isotherm is the best model. This model assumes there is a monolayer

sorption[4]. Although the data shows a good fit to the Langmuir isotherm model, it also shows a good fit with the Freundlich isotherm model and better fits this model theoretically as well. Freundlich assumes a heterogeneity of the surface and active sites and multilayer sorption[4] which is more likely to be the case with PANI.

Table 4.1. *Comparison of Langmuir and Freundlich constants for Ru(III) sorption into PANI.*

Langmuir isotherm	**q**	51
	b	0.32
	R^2	0.99
Freundlich isotherm	**K_f**	0.02
	n	1.01
	R^2	0.99

Taking into account that q_e depends on the initial concentration of $RuCl_3$ in buffer solution, an attempt was made to investigate the sorption rate using the pseudo-second order Lagergren rate equation[58]:

$$\frac{t}{q_t} = \frac{1}{2k' q_e^2} + \frac{t}{q_e} \quad \text{..... (3)}$$

where q_t (mg*g^{-1}) is the sorption capacity of PANI at time t (min) and k' (g*mg^{-1}*min^{-1}) is the rate constant for pseudo-second order sorption. The sorption capacity at equilibrium q_e was determined experimentally. From the linear plot of t/q_t versus t (not shown) the correlation coefficient of R^2=1 was determined. The high correlation coefficient supports the pseudo-second order kinetics and is in agreement with chemisorption being the rate controlling step[58]. The rate constant k' averaged within the tested concentration range was experimentally determined to be 1.3×10^{-2} g*mg^{-1}*min^{-1}. The observed variance in the rate constant k' can be accounted by the inhomogeneity of the sorbent due to PANI particle size distribution.

CHAPTER 5

PHYSICAL AND CHEMICAL STUDY OF SORPTION INTERACTION

5.1 Experimental Techniques used for Characterization

Photoacoustic Spectroscopy (PAS) measurements were carried out using the FTS6000 Spectrometer under helium atmosphere using rapid scan mode at the modulation frequency 2.5 kHz. Dried PANI powder samples were loaded into aluminum pans and scanned over the wave number range of $3500cm^{-1}$ – $800cm^{-1}$. The data was normalized and smoothed using OriginPro 9.0.

X-ray photoelectron spectroscopy (XPS) measurements were carried out using a ThermoFisher Scientific spectrometer with an Al K-alpha X-ray photoelectron source. The instrument was calibrated using a gold (Au) standard giving a binding energy (BE) of 83.96eV for the Au $4f_{7/2}$. The vacuum in the analysis chamber was maintained at $2.5x10^{-8}$ mbar or lower. A flood gun (low energy ionized Ar gas) was used to neutralize the surface charges. Samples were placed in a powder sample holder. Spectra were analyzed using a 400μm X-ray spot size with ThermoScientific Avantage Software. Pass energies of 200 eV for the survey scan and 50 eV for the elemental scans were used.

For Thermal Gravimetric Analysis (TGA), 15-40mg samples of PANI-B, PANI-Ru, and $RuCl_3 \cdot 3H_2O$ were loaded into a platinum crucible and mounted onto the TGA Q-500 from (TA instruments). The samples were heated with scan rates of 20°C/min ranging from 20°C to 800°C under either N_2 or air.

Resonance Raman spectra were collected using a Renishaw inVia Raman Spectrometer coupled onto a Leica DM 2500M microscope containing a 20x / 0.4 N.A. objective and a 1200 lines/nm grating. The measurements were done using a 785nm diode laser with an exposure time between 25-50 seconds. Backscattered signals were

collected in the range of 400-1800cm^{-1} on a CCD detector. The data was normalized and smoothed using OriginPro 9.0.

5.2 Photoacoustic Spectroscopy (PAS) Study

In order to gain more information on the Ru sorption process by PANI-B, structural changes in PANI were compared using PAS (Figure 5.1). The important features are: (1) Over the range of 4000-2000cm^{-1} the baseline became flat when PANI changed from ES to Emeraldine Base (EB) and remained such after Ru sorption (see insert to Figure 5.1). This implies self-localization of electrons along the polymer chain. In the region of 3500-3000cm^{-1} the absorption was rather weak for ES but increased for EB before and after interaction with ruthenium. The peak at 3300cm^{-1} can be attributed to the N-H stretching vibration and a small C-H aromatic stretching vibration was present at the 3050cm^{-1} shoulder[59]. (2) The intensity of all the peaks except for the peak at ~1503cm^{-1} (benzenoid unit C=C stretch)[59] decreased with changing the environment from acid to buffer and later to $RuCl_3$ in buffer. (3) The peaks at ~1590cm^{-1} (quinoid unit C=C stretch)[59] and ~1503cm^{-1} for ES shifted to higher frequency by about 10cm^{-1} when converted to EB and shifted again after ruthenium sorption to lower frequency. This frequency shift of the B and Q units can be attributed to ring stretching in N-B-N and N=Q=N.

In the region from 1400-1240cm^{-1}, the peaks represent the stretching of aromatic amines. Bands at 1311cm^{-1} and 1242cm^{-1} (-C-N stretch) and 1380cm^{-1} (deformation of the C-N bond) were present[60]. The decrease in their intensity indicates that the =NH and –NH structures were involved in the sorption process. The in-plane and out-of-plane bending of the C-H bond in aromatic rings[60] were located in the region of 1220cm^{-1} to 800cm^{-1}. The peak at 1150cm^{-1} was considered by MacDiarmid *et al.*[61, 62] as a measure of the delocalization of electrons on PANI chains that mirrors in the

conductivity. This band is narrower and lower in intensity for EB and remains not changed after Ru sorption. The double peaks at 965cm^{-1} and 950cm^{-1} were assigned to phosphoric acid[26]. The intensity of those peaks at 965cm^{-1}, 950cm^{-1} and 3203cm^{-1} are indicative of $H_2PO_4^-$ anions present in all three forms of PANI. The strong peak centered at 830cm^{-1} was attributed to the out of plane bending of the C-H bond[59].

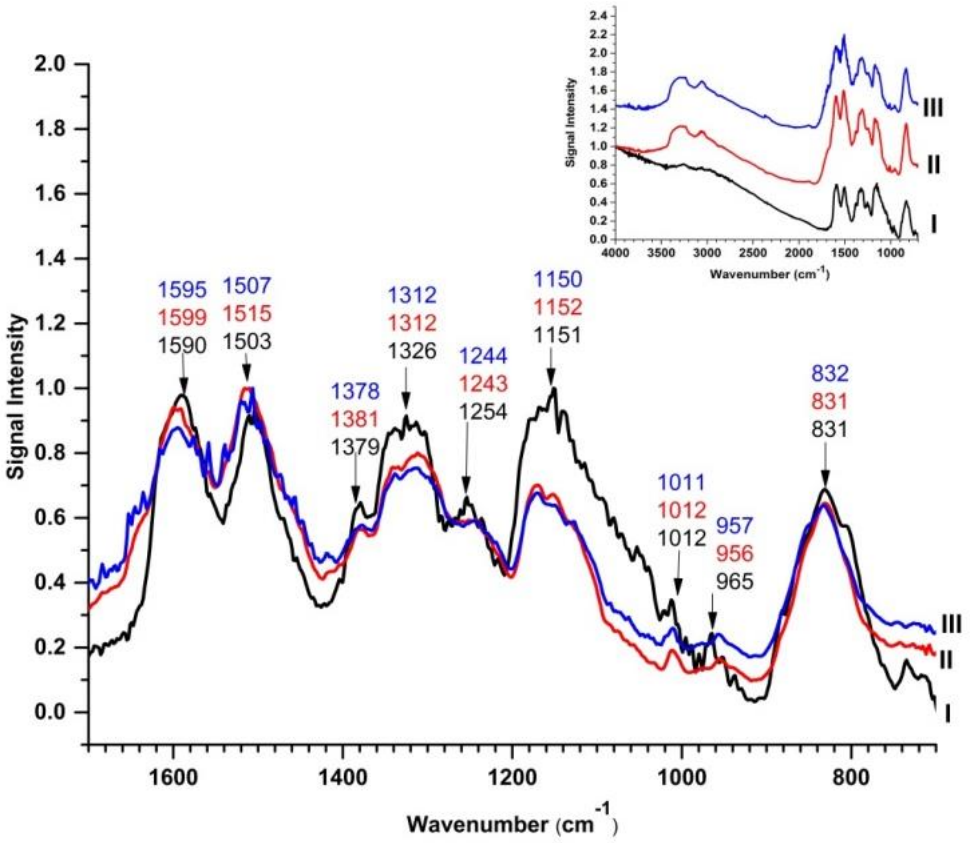

Figure 5.1. *PAS spectra of PANI powder chemically prepared from 3M H_3PO_4 after: (I) synthesis, (II) conditioning to pH 7.0 with phosphate buffer (24 hours), and (III) ruthenium sorption. The extended wavenumber range is shown in the insert.*

5.3 X-ray Photoelectron Spectroscopy (XPS) Study

XPS was used for characterization of electronic and geometric structures of elements in PANI-B and PANI-Ru. Survey of PANI-B contained the presence of C1s (80.85%), N1s (12.34%), and O1s (6.8%), but no clear evidence of phosphorus was observed. In

Figure 5.2A, the survey spectra of PANI-Ru and the relative concentration of core-elements are shown.

The C/N ratio higher than 6 for PANI-B did not change with sorption of ruthenium and can be attributed to degradation products of the PANI[63]. The binding energy overlap of Ru3d and C1s is seen in Figure 5.2B. A peak deconvolution of C1s-Ru3d band was performed by fixing the BE between $Ru3d_{5/2}$ – $Ru3d_{3/2}$ to 4.22eV. Data analysis of the resolved Ru3d doublet ($3d_{5/2}$ and $3d_{3/2}$ at 282.09eV and 286.31eV, respectively) has been assigned to $RuCl_3 \bullet 3H_2O$[64]. The relative amount of Ru3d in the polymer was determined to be 1.89% in the survey, which is consistent with the quantitative sorption results obtained via UV-Vis absorption spectroscopy. In addition, $Ru3p_{3/2}$ at 463.64eV (43.86%), $Ru3p_{1/2}$ at 486.07eV (44.44%), and Ru3p at 467.11eV (11.7%) were analyzed in detail and are presented in Figure 5.2C.

Table 5.1. *High resolution XPS of PANI N1s core orbital.*

PANI-B		**PANI-Ru**	
BE (eV)	**Atomic %**	**BE (eV)**	**Atomic %**
399.71	65.37	400.05	70.73
398.45	20.46	398.88	23.69
401.86	6.46	402.21	2.89
404.97	7.71	403.7	2.69

The shift of N1s core binding energy from 399.8eV (PANI-B) to 400.19eV (PANI-Ru) suggests that the electron density on the nitrogen atom changed after sorption of ruthenium. Structural information for the resulting PANI-Ru sorbent was obtained through deconvolution of the N1s core orbital: –N= (398.88eV), -N- (400.05eV), $-N^+$ (402.21eV), and $=N^+$ (403.70eV), Table 5.1 and Figure 5.2D. The majority of the

polymer consisted of amine units (-N-B-N-) with a smaller portion of the polymer consisting of imine units (-N=Q=N-). The amine to imine ratio remains relatively unchanged when PANI-B was exposed to $RuCl_3$, whereas, the overall protonation of PANI–Ru decreased.

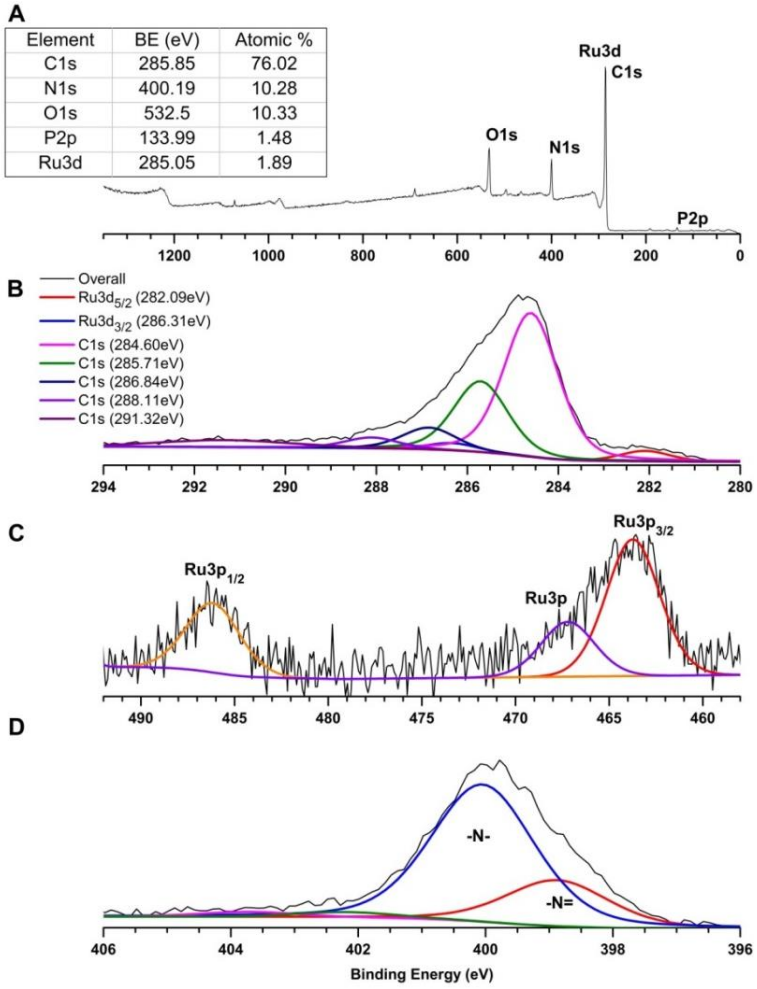

Figure 5.2. *XPS of PANI-Ru: (A) Survey spectrum of core elements with binding energy (BE) and atomic % composition shown in table. (B) High resolution spectra resulting from Ru3d and C1s transitions. (C) Fitted Ru3p spectra. (D) Deconvoluted N1s structural orbital.*

The unprotonated amine and imine groups of the benzenoid units act as Lewis bases, implying the sorption interaction of $RuCl_3$ by PANI is purely Lewis acid-base in nature. As a result of this weak charge-transfer interaction, a partial positive charge is imposed on the polyaniline. This positive charge is delocalized within the polymer chain leading

to polymer chain conformation. It may also be responsible for the presence of 1.48% P2p in the PANI-Ru survey due to insertion of the charge compensating phosphate anions.

5.4 Thermal Stability

It was previously reported that during thermal gravimetric analysis (TGA) the loss of bound and unbound water can be observed[65-67]. Figure 5.3 shows thermograms of PANI-B, PANI-Ru, and $RuCl_3 \cdot 3H_2O$ recorded in air and N_2, respectively. The initial weight loss extending from room temperature up to 130°C for both air and N_2 is due to loss of unbound water molecules from the polymer matrix. In air, the second step between ~130-350°C is due to the loss of bound water. Thermal degradation of the PANI backbone and carbonization of the intermediates takes place between ~300-800°C. In N_2, the thermal decomposition process between 130-450°C is again due to loss of unbound water. For PANI-B, random degradation of the polymer backbone takes place between 450-800°C, whereas the presence of ruthenium (PANI-Ru) raises the activation energy of the PANI degradation process.

Thermograms recorded in air of PANI powder before and after sorption of ruthenium look similar with an overall weight loss at 800°C of ~94%. However, the same materials recorded in N_2 show higher thermal stability when ruthenium is present. The total amount of weight loss at 800°C for PANI-B and PANI-Ru under N_2 was 42% and 26.5%, respectively. The weight loss under nitrogen atmosphere suggests that a crosslinking reaction in the presence of $RuCl_3$ in PANI is more favorable. It was reported that the addition of metals increases the overall thermal stability of the polymer[68-70].

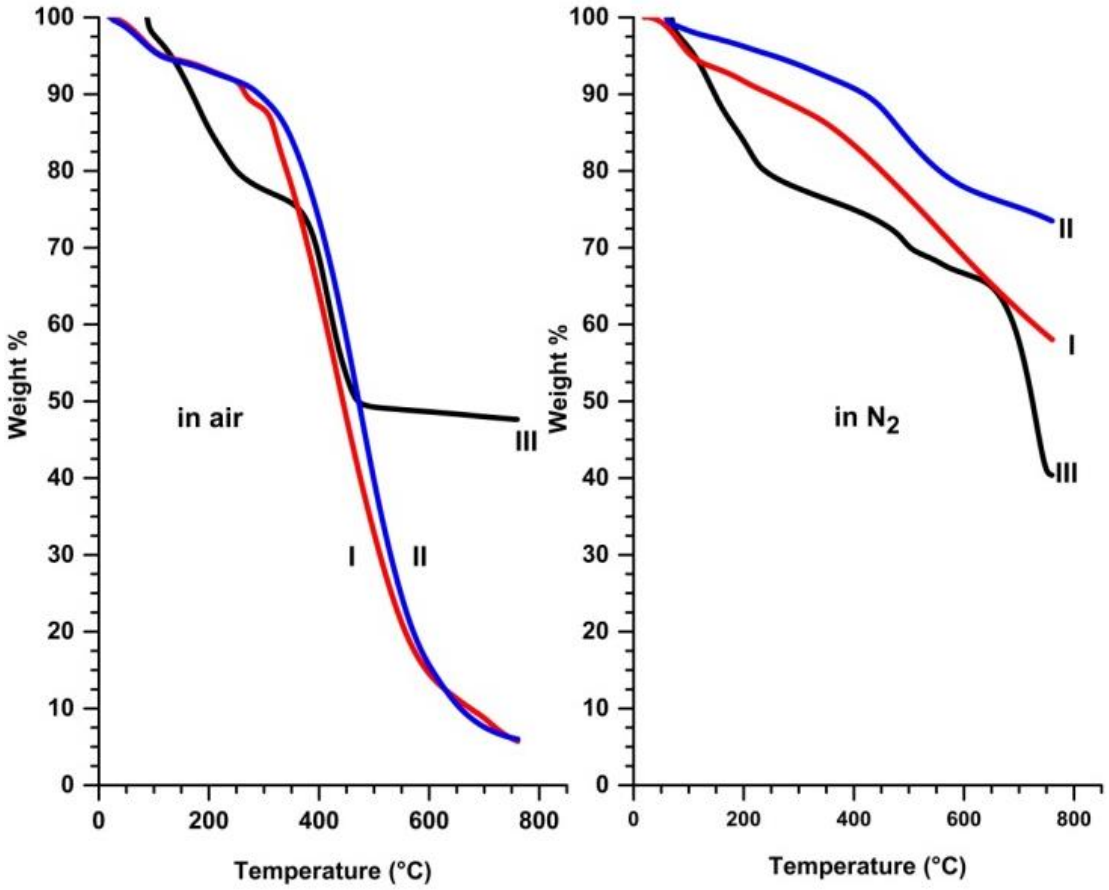

Figure 5.3. *Thermogram of PANI-B powder before (I) and after (II) sorption of ruthenium, PANI-Ru. For comparison, thermograms of $RuCl_3 \cdot 3H_2O$ are also shown (III).*

5.5 Raman studies of the PANI-$RuCl_3$ interaction

Resonance Raman spectroscopy has been employed to explore the intrinsic redox state of PANI after exposure to $RuCl_3$. The spectrum of PANI film polymerized on quartz from 3M H_3PO_4 (PANI-P) was stable in air and is shown in Figure 5.4, curve (I).

Since spectra of both the PANI-B and PANI-Ru films were nearly identical, only the later one is shown in spectrum (II). The spectra (I) and (II) show major differences in the region from 1100-1650cm^{-1}. Because the excitation wavelength at 785nm was used, the benzenoid units were enhanced, especially in the case of the ES form where there is good overlap of the 785nm laser with the molecular absorbance as seen in Figure 4.2.

Semiquinone stretching in the region of 1300-1400cm^{-1} and 1470-1530cm^{-1} is attributed to the C-N$^{+\bullet}$ [71].

The PANI-Ru film after about a week, spectrum (III), has the same characteristic stretches at 585, 710, 810, 1258, 1342, and 1493cm^{-1} as the ES, spectrum (I), that are not seen in the EB form, spectrum (II). The intensity ratio of the stretch at 1322cm^{-1} compared with the reference at 1168cm^{-1} is the same for both spectra (I) and (III) but different for spectrum (II) with ratios of 0.75 and 0.5, respectively. The observed changes for the peak at ~585cm^{-1} correspond to the in-plane amine deformation of the ES[72, 73] seen in spectra (I) and (III). It is not present for the EB form in spectrum (II).

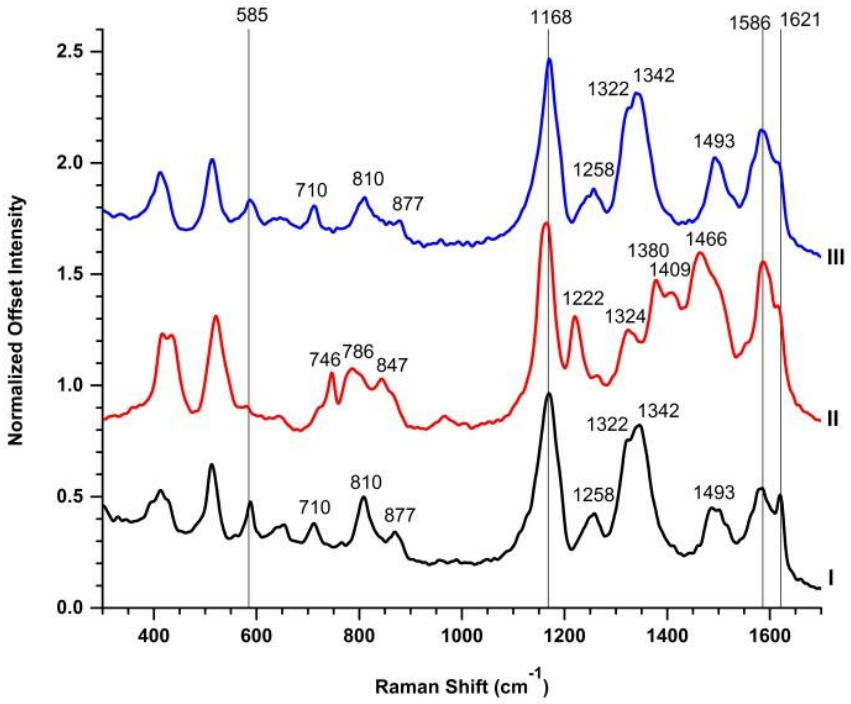

Figure 5.4. *Resonance Raman spectra of PANI film deposited onto a quartz slide: (I) after chemical polymerization in H_3PO_4, PANI-P (II) after 24 hours sorption of PANI-B film in 0.98M $RuCl_3$ in 0.1 M phosphate buffer, and (III) after approximately a week exposure of PANI-Ru film to air.*

The peak at 746cm^{-1} assigned to the imine deformation of the EB form[74] is only present in spectrum (II) of the initial PANI-Ru. This means that the two basic sites, amine and imine, are capable of forming a charge-transfer complex with the Lewis acid. With time this vibration at 746cm^{-1} loses intensity suggesting that some slow intermolecular rearrangements of charge are taking place. Since spectrum (III) resembles spectrum (I) we hypothesize that the PANI matrix can accommodate $H_2PO_4^-$ ions which then can undergo the following reaction, $H_2PO_4^- = H^+ + HPO_4^{2-}$. The freed H^+ in some regions of the PANI may lead to Brønsted type protonation. The charge delocalization process is accompanied by slow rearrangements of polymer chains which are much slower than the Brønsted proton doping. Thus, the slow conductivity increase is assigned to the Lewis-acid charge transfer process. Also, the smaller magnitude of the conductivity change, when compared to the Brønsted acid doped sample (PANI-P), reinforced the differences between them.

CHAPTER 6

CONCLUSIONS AND FUTURE DIRECTIONS

6.1 Concluding Remarks

In summary, polyaniline chemically polymerized from phosphoric acid has been identified spectrophotometrically as emeraldine salt. Upon soaking in 0.1M phosphate buffer at pH 7.0, the proton binding of the amine and imine units to the phosphate anion (Brønsted doping) was weakened. That influences the stabilization of quinoid units in the polymer. The electronic states of PANI-B film correspond to the emeraldine base as seen in the optical spectra. Polyaniline in the EB form was successfully used as a sorbent material for collection of the $RuCl_3 \cdot 3H_2O$ in the 10^{-4}M concentration range. We found that the sorption process was dependent upon the $RuCl_3$/PANI ratio (in mg/g) and followed the Langmuir and Freundlich isotherms. Sorption data was modeled after pseudo-second order kinetics.

The onset of the thermal decomposition of PANI-Ru powder is always higher than of the PANI-B and the overall weight loss for both is higher in air when compared to N_2. The insertion of $RuCl_3$ into the polymer matrix lowers the electron density on the nitrogen atoms and simultaneously imposes a positive charge leading to delocalization of that charge within the polymer chain. This was identified in UV-Vis, PAS, XPS and resonance Raman studies. This type of Lewis charge transfer is attributed to the charge delocalization process. It involves conformational changes in the entire PANI matrix which are very slow and leads to an increase of PANI conductivity.

We have shown that $RuCl_3$ was sorbed by PANI-B through a Lewis-acid based charge transfer interaction. It is important to mention that the Lewis-acid based interaction at pH 7.0 is much slower than the Brønsted doping of polyaniline. This process opens the possibility of using it for removal of trace quantities of ruthenium and

other transition metal complexes by polyaniline, such as in environmentally important systems where the pH is approximately neutral.

6.2 Future Directions

Polyaniline as a sorbent polymer has the ability to be constructed into a micro-column[75] and therefore could be optimized for a new analytical technique of trace radionuclide detection of Ru-106. By incorporating this PANI micro-column (Figure 6.1, (1)) into a SIA system, we can propose to manufacture a robust, portable system for field measurements of environmental samples.

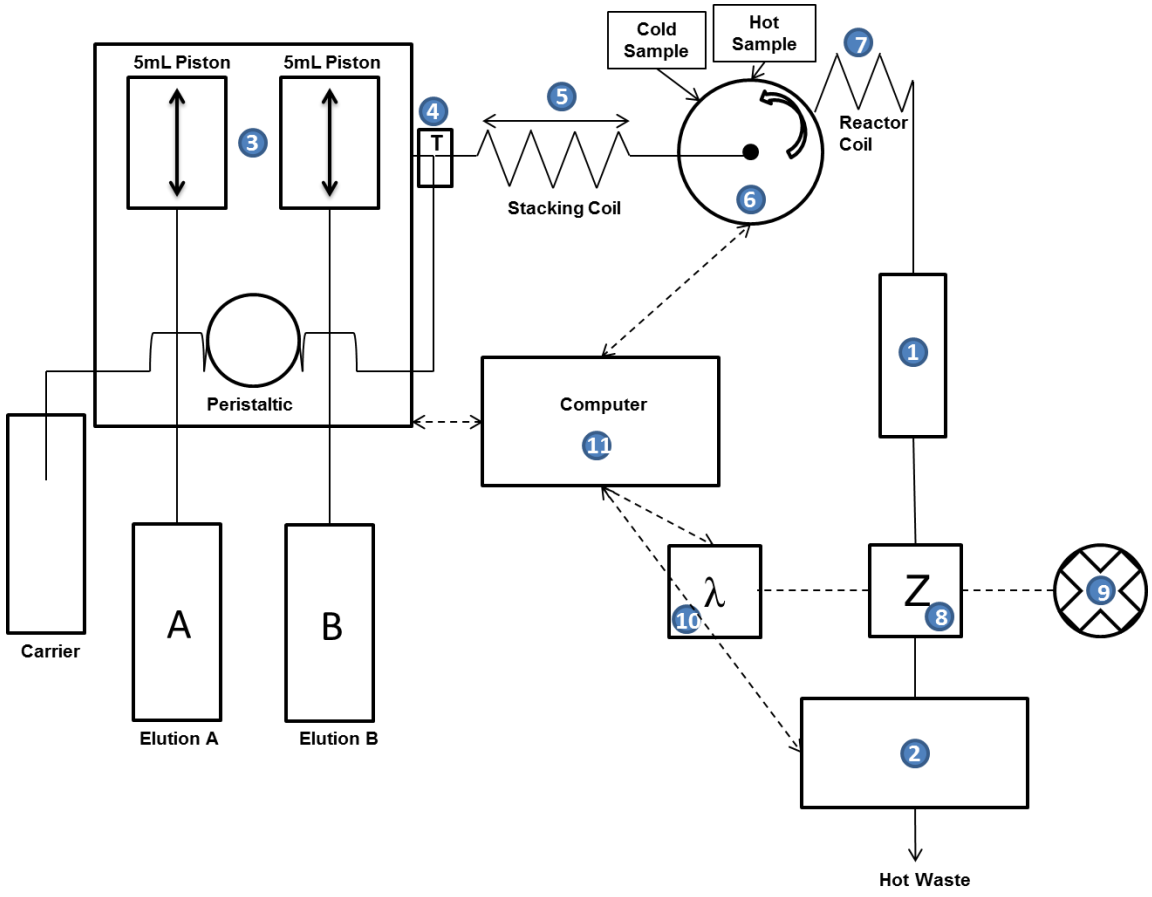

Figure 6.1. *Sequential injection analysis schematic for environmental sample loading, detection, and waste collection.*

The amount of waste (Figure 6.1, (2)) would be minimal due to the small solution volumes required by the SIA system. A carrier solution, such a phosphate buffer, would

flow at a specified rate set by the peristaltic pump to the T junction (Figure 6.1, (4)). Elution A and B would hold solutions to help control the pH through the system and are controlled by piston pumps. The carrier solution would go through the stacking coil (Figure 6.1, (5)) to the sample injection port (Figure 6.1, (6)) where the potentially “hot” radioactive sample would be injected along with a “cold” sample spike for internal calibration of the instrument. The solution would be pushed by the peristaltic pump to the reactor coil (Figure 6.1, (7)) where the solutions would stack in the order of: buffer, environmental sample containing ruthenium, and buffer. This solution would run through the PANI micro-column which collects the ruthenium from solution and the remaining solution would flow through a Z-cell (Figure 6.1, (8)) where the solution would be detected via UV-Vis absorbance (Figure 6.1, (10)) as well as through gamma spectroscopy (Figure 6.1, (9)). This would concentrate the ruthenium to the PANI surface. This could then be eluted from the column and collected in a small concentrated liquid sample. Quantification of ruthenium in solution would again be monitored through UV-Vis absorbance spectroscopy and gamma spectroscopy as the sample is eluted from the column. The SIA system allows for experimental conditions such as concentration and pH of solution to be varied with ease. The experimental design outlined here would be novel for in-field detection of trace radionuclides such as Ru-106.

REFERENCES

1. M. Balcerzak, *Crit Rev Anal Chem*, 2002, **32**, 181-226.

2. M. Y. Suh, C. H. Lee, K. S. Choi, B. C. Song, Y. J. Park and W. H. Kim, *B Kor Chem Soc*, 2002, **23**, 1819-1822.

3. P. Swain, C. Mallika, R. Srinivasan, U. K. Mudali and R. Natarajan, *J Radioanal Nucl Ch*, 2013, **298**, 781-796.

4. S. Sharma, S. K. Ghosh and J. N. Sharma, *Separ Sci Technol*, 2016, **51**, 929-938.

5. T. P. Valsala, M. S. Sonavane, S. G. Kore, N. L. Sonar, V. De, Y. Raghavendra, S. Chattopadyaya, U. Dani, Y. Kulkarni and R. D. Changrani, *J Hazard Mater*, 2011, **196**, 22-28.

6. S. H. Lee and H. Chung, *Separ Sci Technol*, 2003, **38**, 3459-3472.

7. B. R.-D. Zenon Matuszak, Aneta Skwara, Krystyna Urbanska, Maria Starzycka, *Current Topics in Biophysics*, 2000, **24**, 79-82.

8. D. A. Wilkinson, M. Kolar, P. A. Fleming and A. D. Singh, *Brit J Radiol*, 2008, **81**, 784-789.

9. M. F. Chan, A. Y. C. Fung, Y. C. Hu, H. Amols, M. Zaider and D. Abramson, *P Ann Int Ieee Embs*, 2000, **22**, 2431-2432.

10. L. Brualla, J. Sempau, F. J. Zaragoza, A. Wittig and W. Sauerwein, *Strahlenther Onkol*, 2013, **189**, 68-73.

11. S. W. Won, I. S. Kwak, J. Mao and Y. S. Yun, *Industrial & Engineering Chemistry Research*, 2015, **54**, 7148-7153.

12. P. A. Kumar, S. Chakraborty and M. Ray, *Chem Eng J*, 2008, **141**, 130-140.

13. M. R. Samani, S. M. Borghei, A. Olad and M. J. Chaichi, *J Hazard Mater*, 2010, **184**, 248-254.

14. R. K. Gupta, R. A. Singh and S. S. Dubey, *Sep Purif Technol*, 2004, **38**, 225-232.

15. Y. Zhang, Q. Li, L. Sun, R. Tang and J. P. Zhai, *J Hazard Mater*, 2010, **175**, 404-409.

16. R. K. Gupta and S. S. Dubey, *J Polym Res*, 2005, **12**, 31-35.

17. M. V. B. Krishna, J. Arunachalam, D. R. Prabhu, V. K. Manchanda and S. Kumar, *Separ Sci Technol*, 2005, **40**, 1313-1332.

18. S. Kumar, R. Verma and S. Gangadharan, *Analyst*, 1993, **118**, 1085-1087.

19. A. A. Syed and M. K. Dinesan, *React Polym*, 1992, **17**, 145-157.

20. R. Karthik and S. Meenakshi, *Separ Sci Technol*, 2016, **51**, 733-742.

21. J. S. K. Saurabha Bhattarai, Yeoung-Sang Yun, Youn-Sik Lee, *Reactive and Functional Polymers*, 2016, **105**, 52-59.

22. J. Stejskal and R. G. Gilbert, *Pure Appl Chem*, 2002, **74**, 857-867.

23. V. E. Kazarinov, V. N. Andreev, M. A. Spytsin and A. V. Shlepakov, *Electrochim Acta*, 1990, **35**, 899-904.

24. S. L. Mu, Y. Kong and J. Wu, *Chinese J Polym Sci*, 2004, **22**, 405-415.

25. P. Sbaite, D. Huerta-Vilca, C. Barbero, M. C. Miras and A. J. Motheo, *Eur Polym J*, 2004, **40**, 1445-1450.

26. N. V. Blinova, J. Stejskal, M. Trchova and J. Prokes, *Polymer*, 2006, **47**, 42-48.

27. A. Eftekhari and R. Afshani, *J Polym Sci Pol Chem*, 2006, **44**, 3304-3311.

28. L. Brozova, P. Holler, J. Kovarova, J. Stejskal and M. Trchova, *Polym Degrad Stabil*, 2008, **93**, 592-600.

29. H. C. Bajaj and R. Vaneldik, *Inorg Chem*, 1988, **27**, 4052-4055.

30. K. Viljoen, 2003, 1-152.

31. M. M. T. Khan, G. Ramachandraiah and A. P. Rao, *Inorg Chem*, 1986, **25**, 665-670.

32. R. E. Connick and D. A. Fine, *Journal of the American Chemical Society*, 1961, **83**, 3414-&.

33. M. S. Elshahawi, A. Z. Abuzuhri and S. M. Aldaheri, *Fresenius Journal of Analytical Chemistry*, 1994, **350**, 674-677.

34. G. Zotti, S. Cattarin and N. Comisso, *J Electroanal Chem*, 1988, **239**, 387-396.

35. S. P. Armes and J. F. Miller, *Synthetic Met*, 1988, **22**, 385-393.

36. C. Dalmolin, S. R. Biaggio, R. C. Rocha and N. Bocchi, *J Solid State Electr*, 2007, **11**, 609-618.

37. E. M. Genies, M. Lapkowski and J. F. Penneau, *J Electroanal Chem*, 1988, **249**, 97-107.

38. F. Genoud, I. Kulszewicz-Bajer, A. Bedel, J. L. Odbou, C. Jeandey and A. Pron, *Chem Mater*, 2000, **12**, 744-749.

39. C. M. S. Izumi, A. M. D. C. Ferreira, V. R. L. Constantino and M. L. A. Temperini, *Macromolecules*, 2007, **40**, 3204-3212.

40. O. P. Dimitriev and V. V. Kislyuk, *Synthetic Met*, 2002, **132**, 87-92.

41. O. P. Dimitriev, P. S. Smertenko, B. Stiller and L. Brehmer, *Synthetic Met*, 2005, **149**, 187-192.

42. O. P. Dimitriev, *Macromolecules*, 2004, **37**, 3388-3395.

43. M. Higuchi, D. Imoda and T. Hirao, *Macromolecules*, 1996, **29**, 8277-8279.

44. M. Hasik, I. Kurkowska and A. Bernasik, *React Funct Polym*, 2006, **66**, 1703-1710.

45. F. Genoud, I. Kulszewicz-Bajer, B. Dufour, P. Rannou and A. Pron, *Synthetic Met*, 2001, **119**, 415-416.

46. S. J. Choi and S. M. Park, *J Electrochem Soc*, 2002, **149**, E26-E34.

47. I. Sapurina and J. Stejskal, *Polym Int*, 2008, **57**, 1295-1325.

48. A. G. Macdiarmid, J. C. Chiang, W. S. Huang, B. D. Humphrey and N. L. D. Somasiri, *Mol Cryst Liq Cryst*, 1985, **125**, 309-318.

49. J. C. Chiang and A. G. Macdiarmid, *Synthetic Met*, 1986, **13**, 193-205.

50. A. G. Macdiarmid, J. C. Chiang, A. F. Richter and A. J. Epstein, *Synthetic Met*, 1987, **18**, 285-290.

51. W. W. Focke, G. E. Wnek and Y. Wei, *J Phys Chem-Us*, 1987, **91**, 5813-5818.

52. P. M. Mcmanus, S. C. Yang and R. J. Cushman, *J Chem Soc Chem Comm*, 1985, DOI: DOI 10.1039/c39850001556, 1556-1557.

53. M. Nechtschein, C. Santier, J. P. Travers, J. Chroboczek, A. Alix and M. Ripert, *Synthetic Met*, 1987, **18**, 311-316.

54. J. P. Travers and M. Nechtschein, *Synthetic Met*, 1987, **21**, 135-141.

55. M. Angelopoulos, A. Ray, A. G. Macdiarmid and A. J. Epstein, *Synthetic Met*, 1987, **21**, 21-30.

56. A. P. Monkman, D. Bloor, G. C. Stevens, J. C. H. Stevens and P. Wilson, *Synthetic Met*, 1989, **29**, E277-E284.

57. M. S. Mansour, M. E. Ossman and H. A. Farag, *Desalination*, 2011, **272**, 301-305.

58. Y. S. Ho and G. McKay, *Process Saf Environ*, 1998, **76**, 332-340.

59. D. W. Hatchett, M. Josowicz and J. Janata, *J Phys Chem B*, 1999, **103**, 10992-10998.

60. G. Inzelt and Z. Puskas, *J Solid State Electr*, 2006, **10**, 125-133.

61. J. S. Tang, X. B. Jing, B. C. Wang and F. S. Wang, *Synthetic Met*, 1988, **24**, 231-238.

62. T. Hjertberg, W. R. Salaneck, I. Lundstrom, N. L. D. Somasiri and A. G. Macdiarmid, *J Polym Sci Pol Lett*, 1985, **23**, 503-508.

63. F. J. Liu, L. M. Huang, T. C. Wen and A. Gopalan, *Synthetic Met*, 2007, **157**, 651-658.

64. A. K.-V. Alexander V. Naumkin, Stephen W. Gaarenstroom, and Cedric J. Powell, NIST Standard Reference Database 20, Version 4.1, http://srdata.nist.gov/xps/Default.aspx, (accessed May 24, 2016).

65. S. Bhadra and D. Khastgir, *Polym Degrad Stabil*, 2008, **93**, 1094-1099.

66. K. Luo, N. L. Shi and C. Sun, *Polym Degrad Stabil*, 2006, **91**, 2660-2664.

67. C. M. Yang, Z. Fang, J. B. Liu, W. P. Liu and H. Zhou, *Thermochim Acta*, 2000, **352**, 159-164.

68. S. Giri, D. Ghosh and C. K. Das, *Nano*, 2013, **8**.

69. W. M. Millan and M. A. Smit, *J Appl Polym Sci*, 2009, **112**, 2959-2967.

70. W. M. Millan, T. T. Thompson, L. G. Arriaga and M. A. Smit, *Int J Hydrogen Energ*, 2009, **34**, 694-702.

71. Y. Furukawa, F. Ueda, Y. Hyodo, I. Harada, T. Nakajima and T. Kawagoe, *Macromolecules*, 1988, **21**, 1297-1305.

72. M. Trchova, Z. Moravkova, I. Sedenkova and J. Stejskal, *Chem Pap*, 2012, **66**, 415-445.

73. C. Liu, J. X. Zhang, G. Q. Shi and F. E. Chen, *J Appl Polym Sci*, 2004, **92**, 171-177.

74. T. Lindfors and A. Ivaska, *J Electroanal Chem*, 2005, **580**, 320-329.

75. M. V. B. Krishna, K. Chandrasekaran and D. Karunasagar, *Talanta*, 2010, **81**, 462-472.